Master's thesis
Master's Programme in Particle Physics and Astrophysical Sciences

Quality Assurance of Diamond Radiation Detectors

Milla-Maarit Rantanen

June 2020

Supervisor(s): PhD Erik Brücken
PhD Vladyslav Litichevskyi
prof. Kenneth Österberg

Censor(s): prof. Kenneth Österberg
PhD Erik Brücken

UNIVERSITY OF HELSINKI
Department of physics

P.O. Box 64 (Gustaf Hällströmin katu 2a)
FI-00014 University of Helsinki

HELSINGIN YLIOPISTO — HELSINGFORS UNIVERSITET — UNIVERSITY OF HELSINKI

Tiedekunta — Fakultet — Faculty	Laitos — Institution — Department
Faculty of Science	Department of physics

Tekijä — Författare — Author

Milla-Maarit Rantanen

Työn nimi — Arbetets titel — Title

Quality Assurance of Diamond Radiation Detectors

Koulutusohjelma — Utbildningsprogram — Degree programme

Master's Programme in Particle Physics and Astrophysical Sciences

Työn laji — Arbetets art — Level	Aika — Datum — Month and year	Sivumäärä — Sidoantal — Number of pages
Master's thesis	June 2020	77 pages

Tiivistelmä — Referat — Abstract

Halvledarstrålningsdetektorer är anordningar menade för detektering av elektromagnetisk strålning och partikelstrålning. Signalformationen i dem baserar sig på transport av laddningar mellan valens- och ledningsbanden. Växelverkan mellan detektormaterialet och strålningen producerar fria negativt laddade elektroner och positivt laddade hål som rör sig i motsatt riktning i elfältet mellan detektorns elektroder. Rörelsen inducerar en ström i den yttre elkretsen, som kan användas för identifiering av partikelstrålning, bestämning av deras energi eller rörelsemängd, samt deras bana.

Det finns många olika detektormaterial och -system, och nya planeras hela tiden. Ett material som har väckt intresse inom flera olika områden är diamant. Diamantdetektorer är ett lockande alternativ för flera olika applikationer tack vare sina unika egenskaper. Många av dessa egenskaper härstammar från diamantens kristallstruktur och styrkan hos bindningarna mellan kolatomerna. Den täta och rigida strukturen gör diamant till ett hårt och hållbart material, vilket möjliggör användningen av diamantdetektorer i krävande strålningsförhållanden. Detta kombinerat med snabba transporten av laddingar och den korta responstiden gör diamantdetektorer ett utmärkt val för tillämpningar inom högenergifysik. Diamantens kristallstruktur leder också till ett brett bandgap. Tack vare det breda bandgapet har diamantdetektorer liten läckström och de kan användas t.o.m. vid höga temperaturer utan skydd för omgivande ljus.

Speciellt de elektriska egenskaperna hos halvledare beror starkt på mängden orenheter och kristalldefekter. Därmed är bestämningen av de elektriska egenskaperna ett bra sätt att få en bild av kristallens kvalitet. Materialets elektriska egenskaper bestämmer spänningsområdet inom vilket anordningen kan användas på ett säkert sätt, och för optimerad användning av halvledardetektorer behövs kunskap om anordningens läckström och transportmekanismerna för elektroner och hål. Därför är karakterisering av materialets egenskaper en viktig del av framställningen av halvledaranordningar. Karakterisering bör göras i olika skeden av framställningen för att märka när eventuella problem uppstått och lättare förstå orsaken till dem. I det här arbetet beskrivs processen för kvalitetskontrollen av singlekristall CVD (kemisk förågningssdeposition, chemical vapour deposition) diamantdetektorer för CMS-experimentets PPS-detektor.

Processen inkluderar visuell inspektion av diamantens ytor och dimensioner m.h.a. optiskt och korspolariserat ljus mikroskop, samt elektrisk karakterisering genom mätning av läckström och laddningsinsamlingseffektivitet (CCE, charge collection efficiency). CCE mätapparaturen förbättrades med en styrbar plattform, som möjliggör automatisk mätning av diamanten i flera positioner. Den nya apparaturens funktion och resultatens upprepbarhet undersöktes via upprepade mätningar av en referensdiamant. Mätapparaturen kunde framgångsrikt användas för att mäta CCE över hela diamantens yta. Resultatens osäkerheter är dock stora. Resultaten var stabila och liknande för de olika mätpunkterna. Ytterligare arbete krävs för att minska mätningarnas osäkerhet och för att klargöra korrelationen mellan observerade defekter och mätta elektriska egenskaper.

Avainsanat — Nyckelord — Keywords

radiation detectors, diamond detectors, CVD diamond, electrical characterization

Säilytyspaikka — Förvaringsställe — Where deposited

Muita tietoja — övriga uppgifter — Additional information

Contents

1 Introduction **1**

1.1 Diamond detectors in TOTEM and CMS 2

1.2 Scope of this thesis 4

2 Semiconductor radiation detectors **5**

2.1 Generation of charge carriers in semiconductor materials 6

2.2 Operational principle of semiconductor radiation detectors 9

2.3 Radiation damage 12

3 Diamond radiation detectors **15**

3.1 Classification of diamond 19

3.2 CVD diamond 21

3.3 Polycrystalline and single crystal diamond 23

3.4 Structure of diamond detectors 24

4 Defects **28**

4.1 Effect on semiconductor properties 30

4.2 Defects in diamond 34

5 Characterization **35**

5.1 Visual inspection 35

5.2 Leakage current 38

5.2.1 Measurement of leakage current 39

5.3 Charge collection distance and efficiency 41

5.3.1 Measurement of charge collection distance and efficiency . . . 43

5.3.2 Measurement setup and process 45

6 Results **50**

6.1 Quality assurance measurements 60

6.2 Reducing the measurement uncertainty 64

7 Conclusions 68

Bibliography 70

A Stage controller 75

B Reproducibility measurements 77

1. Introduction

Radiation detectors are devices used to detect electromagnetic and particle radiation. Different detector systems can be built depending on the goal of the measurement. Detector systems can be used for particle identification, measurement of energy or momentum, timing, or tracking. Operation of radiation detectors is based on the interaction of the ionizing radiation with the detector medium, which can be liquid, gas or solid. This thesis studies solid semiconductor detectors. In semiconductor detectors information about the traversing radiation is deduced from the current generated by the movement of charge carriers produced by the radiation.

Semiconductor detectors are used in many fields in science and technology, for example medicine, particle and nuclear physics, energy production, material characterization and imaging in astronomy. Their wide use is due to some unique advantages over other detector types. These advantages include good energy resolution, precise position measurements, small size and relatively fast response. In addition, semiconductor detectors are mechanically rigid so they don't need support structures, and the detector thickness can be changed according to application requirements. However, semiconductor detectors are more expensive and their use is sometimes limited by the small size. Also, many semiconductor materials are relatively sensitive to radiation damage.

There are several options for detector designs and material, and new options are continuously developed and studied. One detector material that has obtained a large amount of interest in many fields is artificial diamond grown by chemical vapor deposition (CVD). This is due to the many unique properties of diamond, such as low leakage current, fast response, the combination of low electrical conduction and high thermal conduction, and radiation tolerance. The radiation tolerance is a particularly intriguing property, since it means that the detector can be operated for a long time without significant changes in the response.

Key factors in semiconductor detector operation is a perfect crystal structure and the energy bands resulting from the formation of a crystal lattice. Small concentrations of impurities and irregularities in the crystal structure can have a significant effect on semiconductor properties, such as charge carrier mobility,

conductivity and charge carrier lifetime. These properties define the safe operational region of the device, and affect the detector operation and stability. Optimal operation of a detector requires knowledge of these properties, which is why characterization, especially determination of electrical properties, is an important part of detector fabrication and system design. This thesis describes characterization of CVD diamond detectors designed for the Precision Proton Spectrometer (PPS) detectors for the CMS-experiment at CERN.

1.1 Diamond detectors in TOTEM and CMS

Diamond detectors are used as time-of-flight detectors in the CMS-TOTEM Precision Proton Spectrometer (CT-PPS) timing layer and in TOTEM timing. The detectors measure the time-of-flight from the point of collision of proton beams colliding in the Large Hadron Collider (LHC) to the detector location inside the Roman Pots (RP) about 200 m from the interaction point. RPs are movable devices consisting of vacuum vessels called pots, detectors for tracking and timing, and vacuum bellows for connecting the pot to the beam line vacuum.[1–3] The detectors are designed to measure inelastic, elastic and total cross sections of proton-proton collisions. Together with the CMS detectors they are used to study diffractive dissociation and central exclusive processes at the LHC.[4] The time-of-flight measurements make it possible to determine the longitudinal position of the proton interaction point and to associate it with one of the vertices that the CMS detectors have reconstructed even when events are piled-up. In case of event pile-up, the timing detectors can be used to determine the difference in arrival time, which is directly proportional to the longitudinal position of the collision point. The difference in arrival time can be used to determine the position of the interaction vertex with an accuracy of a few cm even when several protons are detected at once.[3,4]

The timing detectors need to have timing precision less than 100 ps and excellent efficiency. Also, the detector system for the timing has to be small due to the limited space in the RP. These requirements can be met with single crystal CVD diamond.[4] Besides fast signal properties, diamond is more radiation tolerant than many other detector materials. Both detectors and electronics need to be radiation tolerant in order to provide precise information in the harsh radiation environments of high energy physics experiments.[1,2,5] Silicon, which is a widely used detector material, has very mature processing technology, but it does not have good enough radiation tolerance to withstand the harsh environments, even though its radiation hardness

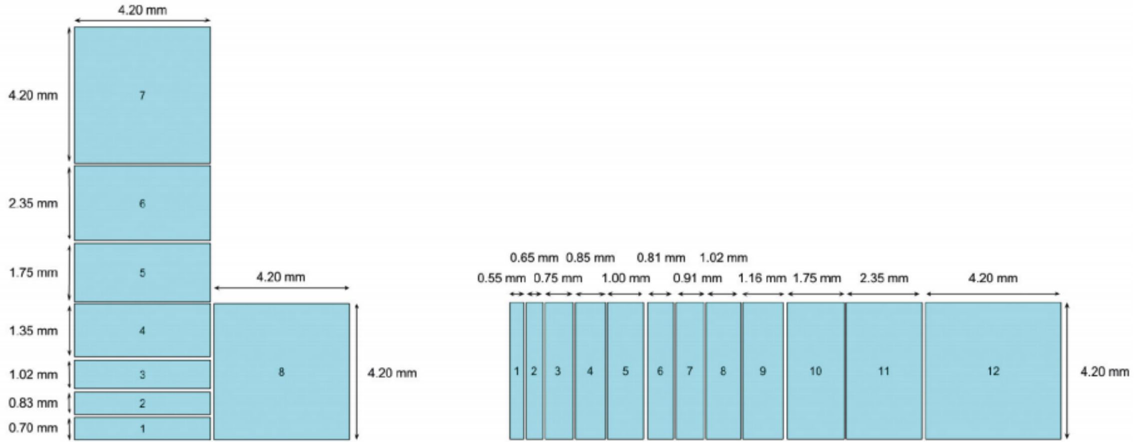

Figure 1.1: Segmentation of the detector planes in the vertical Roman Pot (left) and the CT-PPS (right). Image source [4]

can be increased by different processing methods.[6] Irradiation studies have shown that diamond detectors can be operated for years with high efficiency and good spatial resolution close to the interaction region in the LHC, making it well suited for particle detection in high energy physics.[2,5] The radiation tolerance combined with the fact that CVD diamond can be produced in thicknesses of several hundred µm make it possible to produce self supporting detector systems that can be installed close to the interaction position in particle colliders. The low dielectric constant, small leakage current, the radiation hardness and fast response are the reasons why diamond detectors have found their way into experiments in the LHC.[2,7]

The TOTEM-experiment consists of two sets of detectors placed symmetrically around the interaction point. Each set originally consisted of a RP system, and T1 and T2 telescopes. The T1 telescope consisting of Cathode Strip Chambers was later removed and no upgrades have been planned. The T2 telescope was previously built of Gas Electron Multipliers, but these have now been replaced with segmented plastic scintillators. Both telescopes detect charged particles in the forward region. The RP system consists of two RP stations installed 210 m and 220 m from the interaction point. The stations consists of 2 units consisting of 3 RPs, one horizontal and two vertical. One RP is used for timing and the other two, placed on opposite sides of the timing RP, are used for tracking of leading protons. The RPs housing the timing detectors for the CT-PPS are installed in the RP station at 220 m between the two units described earlier. In the latest upgrade a second timing RP will be built in each RP unit.[3,4,8]

Detectors for tracking were previously edgeless silicon detectors, but these have been gradually replaced with 3D silicon pixel detectors. Timing measurements are

done with single crystal CVD diamond detectors. In year 2017 one diamond detector plane was temporarily replaced with a ultrafast silicon detector (UFSD). The timing detectors in TOTEM are installed in the vertical RPs, and the ones of CT-PPS in the horizontal RPs. Each Roman Pot unit has four segmented sensor planes for timing. Dividing the detector system into four planes improves the precision of the measurement, while segmenting improves the spatial resolution. Segmenting also reduces event pile-up. The detector geometry for TOTEM consists of twelve detector pads with different thickness, arranged so that the thinner pads are in the high activity area. Each detector plane is segmented as shown on the left in Figure 1.1 and consists of eight single crystal CVD diamond detectors. In the detector geometry for the CT-PPS each plane is divided into twelve segments as shown on the right in Figure 1.1.[3,4,8] In order to improve the time resolution, the diamonds of CT-PPS are gradually being changed to double-diamond structures. Half of the diamond planes had been changed to double-diamond in 2018.[9] The signals are read out using dedicated fast low noise electronics.[3]

1.2 Scope of this thesis

This thesis presents the quality assurance of CVD diamond detectors during their fabrication process. All measurements were done at the University of Helsinki. The electrical measurements were done with measurement setups in the Detector Laboratory. The setup for the charge collection efficiency (CCE) measurement was improved to allow automatic and repeatable measurements of several samples at the same time. The visual inspections were done with an optical microscope in the Detector Laboratory and with a cross polarized light microscope in the Geology Laboratory. This thesis describes the quality assurance process and measurements. The focus is on the CCE measurements and the improvements made to the setup.

The structure of this thesis is as follows. Chapter 2 explains important concepts of semiconductor physics and the operational principle of semiconductor radiation detectors. Diamond as detector material, as well as the production of CVD diamond and diamond detectors are presented in Chapter 3. Chapter 4 describes different types of defects present in crystalline materials and their effect on semiconductor properties. The quality assurance process and the measurements are described in Chapter 5. Finally, Chapters 6 and 7 present and discuss the obtained results. Chapter 6 includes also the efforts to reduce the measurement uncertainty.

2. Semiconductor radiation detectors

This chapter presents the basic operational principles of semiconductor radiation detectors, explaining generation of charge carriers in the detector and the signal formation. Discussion about radiation damage and its effects on detector operation is also included. The chapter is based on books by Lutz [10] and Knoll [11]. Additional sources are mentioned when they are used.

For understanding operation of semiconductor detectors, is it important to have some knowledge about semiconductor physics, especially the concept of energy bands. The energy bands are a result of the periodicity of the crystal lattice and they determine where the electrons can be found within the lattice. The formation of these bands can be explained by imagining that crystal lattices consist of atoms that were originally far apart. Atoms that are far apart have the same discrete energy levels and they will not influence each other. But when N number of atoms are brought closer to form a lattice, their energy levels start to overlap. The Pauli exclusion principle states that two electrons can not be in the same quantum state. Therefore the atomic energy levels split into N closely packed molecular energy levels. When $N \to \infty$ the space between each energy level becomes very small and the energy levels become energy bands. As the distance between atoms is reduced, the energy levels overlap more, which leads to broadening of the energy bands. If the distance is reduced further the bands merge before they split again to a lower and upper energy band. The separation between the bands in a material depends on the distance between the atoms.

The band with higher energy is called the conduction band and the band with lower energy the valence band. The valence band corresponds to the electrons that are bound to specific sites in the crystal lattice, while the conduction band corresponds to the electrons that are free to migrate through the crystal and contribute to the electrical conductivity of the material. The conduction and valence band are separated by a band gap (E_g). Because the band gap is forbidden for electrons, those can only be found in the energy bands. The size of the band gap determines whether the material is an insulator, conductor or semiconductor. Insulators have a large band gap, typically 5 eV or more, and conductors have either a partially

filled conduction band or overlapping bands. Semiconductors are something between conductors and insulators. In semiconductors the energy bands are separated, but the band gap is smaller than in insulators. The band gap is typically less than 2 eV, which means that charge carriers can be thermally excited and cross the band gap from the valence band to the conduction band. Figure 2.1 shows the energy bands of insulators, conductors and semiconductors. The dotted area represents bands that are filled with electrons.

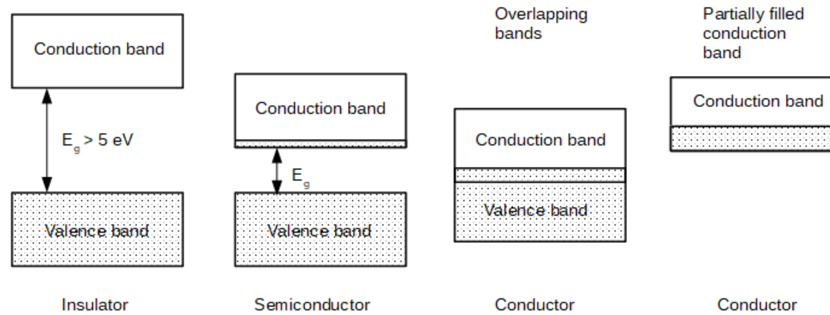

Figure 2.1: Energy bands of insulators, semiconductors and conductors.

2.1 Generation of charge carriers in semiconductor materials

At low temperatures electrons are bound to their lattice sites leading to a completely full valence band and an empty conduction band. At higher temperatures thermal vibrations can break covalent bonds and electrons can be excited to the conduction band. The probability of excitation is small in materials with large band gap and high in materials with small band gap. Each electron excited to the conduction band will leave one hole on the valence band. Both the electron and hole are available for conduction. The probability for thermal excitation depends on the temperature and the size of the band gap. The probability increases with decreasing band gap and increasing temperature. Materials with low probability of excitation will have few electrons on the conduction band and low conductivity, while materials with high excitation probability will have many electrons on the conduction band and high conductivity.

Thermal generation of charges means that semiconductor detectors show some conductivity and steady state leakage current even in absence of ionizing radiation when an electric field is applied over the device. Leakage current and its fluctuations

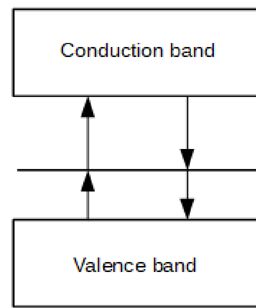

Figure 2.2: Excitation of charge carriers through intermediate energy levels within the band gap.

are a source of noise superimposed on the signal and lead to signal blurring, which have a detrimental effect on semiconductor detector operation. In semiconductors with small band gap thermal generation of charges leads to such large leakage currents that they can not be properly operated in normal room temperature without cooling. The leakage current of a device can be reduced with structures like the reversed biased PN-junction.[12,13] Materials with large band gap can show leakage current even in lower temperatures than the band gap suggests in case there are intermediate energy levels inside the band gap, e.g. due to impurities. These energy levels allow excitation of charges to the conduction band with energy less than the band gap energy. The excitation of charge carriers through intermediate energy levels is illustrated in Figure 2.2.

In radiation detectors one is interested in the number of charge carriers produced by radiation hitting the detector.[14] The operation of any type of radiation detector is based on interactions between the detector material and the studied radiation. Therefore, knowledge of how radiation interacts with matter is a central part of understanding the operation of radiation detectors. Photons interact with matter mainly through photoelectric absorption, Compton scattering and pair production, see Figures 2.3a-2.3c.[15] Photons are absorbed in the detector and the energy they deposit is used to excite valence electrons to the conduction band. If the absorbed photon has energy higher than the band gap, the excess energy is emitted as lattice vibrations (phonons) or lower energy photons. Photons with energy smaller than the band gap can also be absorbed if there are suitable intermediate states within the band gap. Electrons interact with matter mainly through excitation, ionization, Coulombic interactions and radiative losses, called bremsstrahlung. Bremsstrahlung is the emission of photons during deceleration of electrons in their interactions with atomic nuclei, see Figure 2.3d.[15] The total energy deposition is the sum of all these processes. Because electrons have the same mass as orbital electrons, they will

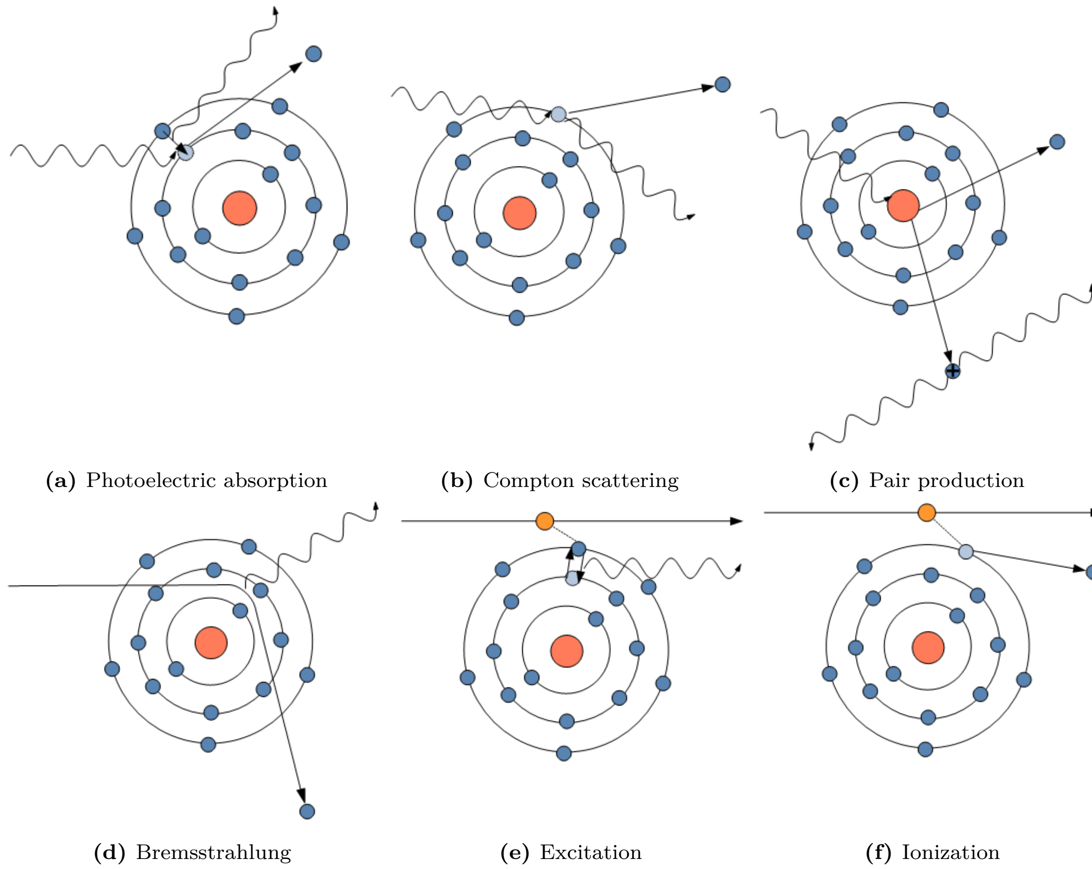

(a) Photoelectric absorption (b) Compton scattering (c) Pair production

(d) Bremsstrahlung (e) Excitation (f) Ionization

Figure 2.3: Mechanisms by which radiation interacts with matter.

scatter in different angles in the interactions and their paths can be very non-linear.

Charged particles deposit their energy mainly through Coulombic interactions with orbital electrons. In each interaction the particle delivers part of its energy to the electrons and slows down. The energy deposition can either lead to excitation of electrons or ionization of atoms, see Figures 2.3e-2.3f. If the electrons obtain large enough energy they can cause further ionization. These electrons are called delta rays. Delta rays have short range and will not travel far from the primary particle track. The energy deposition of charged particles is described by the Bethe-Bloch formula. The formula gives the energy (dE_{p}) deposited per path length dx, called specific energy loss.

$$-\frac{dE_{\mathrm{p}}}{dx} = \frac{4\pi e^4 z^2}{m_0 v} NZ \left[\ln \frac{2m_0 v^2}{I_0} - \ln\left(1 - \frac{v^2}{c^2}\right) - \frac{v^2}{c^2}\right] \tag{2.1}$$

In the formula v is the primary particle velocity and ze is its charge, N is the number density of the absorbing material and Z is atomic number. The electron mass is denoted by m_0, speed of light by c, and the elementary charge by e. I_0 is the average

ionization and excitation potential which is experimentally determined for an element. At low particle energies the energy deposition is inversely proportional to the square of the velocity. The energy deposition decreases rapidly with increasing velocity. When the velocity approaches the speed of light (about $0.95c$ [14]) the energy deposition reaches a near constant minimum. Charged particles reach this minimum when their energy is several hundreds of MeV and electrons when their energy is around 1 MeV. At this point the particles are called minimum ionizing particles (MIP). Further increase of the particle velocity leads to a logarithmic increase in the energy deposition, until it saturates due to polarization of the absorbing material.[14] When the energy deposition of charged particles is large the energy loss is well described by the Bethe-Bloch formula in the form given above. However, if the energy deposition is low, e.g. in thin detectors in which particles deposit only part of their energy, additional terms need to be added to account for the high energy tail of the energy distribution. Additional terms are also needed if delta electrons are able to leave the detector without depositing all of their energy.[13,14] The Bethe-Bloch formula also fails to describe the energy deposition of very low energetic charged particles, for which charge exchange with the absorbing material becomes important.

2.2 Operational principle of semiconductor radiation detectors

Interactions between ionizing radiation and matter lead to formation of electron-hole pairs in the detector active volume. The operational principle of semiconductor detectors is based on collection and measurement of charge carriers along the particle track. The number of generated electron-hole pairs depends on the energy required to form one pair, which in turn depends on the size of the band gap. The number of produced electron-hole pairs depends on the amount of energy deposited by the traversing radiation.[14–18]

After their formation charge carriers undergo random thermal motion within the lattice. The motion is driven by differences in charge concentrations between regions in the lattice.[15,16] The probability for a carrier to move is the same in all directions, so the mean distance carriers travel is zero and charges quickly disappear by recombination if no external electric field is applied.[14,15] However, there is a probability for the carrier to move between regions with different charge concentration. The probability for charges to move from the high concentration region to the lower concentration region is higher so diffusion leads to smoothing of charge carrier

differences. The charge carrier flux ($\mathbf{F}$) due to diffusion is described by

$$\mathbf{F} = -D\nabla q, \tag{2.2}$$

where ∇q is the concentration gradient and D the diffusion coefficient. The diffusion coefficient is related to charge carrier mobility μ.

$$D = \mu \frac{kT}{e} \tag{2.3}$$

Here k is the Boltzmann's constant and T the absolute temperature. Mobility describes how fast carriers travel across the device. Materials with high mobility will hence have fast response. The mobility depends on both temperature and defect concentration. Defects introduce scattering sites that reduce the drift velocity.[19] Because of diffusion charges do not move in a straight line to the electrodes from their point of origin. Charges arrive at the electrodes at slightly different positions, which limits position measurements and leads to broadening of the charge collection time. In many cases the effects of diffusion are so small that they can be neglected, but in detectors with large volume, and in timing or position measurements such effects can be significant.

Voltage is applied to the detector to generate a drift field and to remove free charge carriers. Even when an electric field is applied across the detector some free carriers will be present in the detector volume due to thermal generation of charges, but these quickly drift to the electrodes.[13,17] Generated electrons and holes will drift in opposite directions in the field with mean velocity v.[16] During their drift, carriers will collide with lattice atoms. Between every collision the charge carriers will accelerate due to the influence of the electric field. The mean drift velocity is determined by the electric field strength and number of interactions between carriers and lattice atoms.[14] When the time between collisions is independent of the applied electric field, and the energy carriers obtain in the acceleration is small compared to the thermal energy, the drift velocity will increase linearly with increasing electric field strength. The drift velocity v is given by

$$v = \mu E, \tag{2.4}$$

where E the electric field. [20]

However, at high field strengths the linear relation doesn't apply anymore. Charge carriers undergo more collisions with lattice atoms, and the energy they

obtain in the acceleration becomes large compared to the thermal energy. The velocity increases more slowly with increasing field strength, until it saturates and becomes independent of the applied electric field. In the non-linear region the drift velocity follows the empirical formula

$$v = \frac{\mu_0 E}{1 + \frac{E\mu_0}{v_{\mathrm{sat}}}}, \tag{2.5}$$

where μ_0 is the low field mobility and v_{sat} the saturation drift velocity.[17,20]

Electrons and holes will migrate in opposite directions in the electric field applied across the detector until they are collected at the electrodes. The time it takes to collect the charges depends on the distance carriers have to travel before reaching the electrodes, and on the carrier mobilities.[14,17,18] The movement of charges induces a current at the electrodes.[21,22] Both drift and diffusion contribute to the current generation, and the current lasts until all charge carriers are collected. Electrons and holes have different mobility, so the carrier types will have slightly different collection times.[14] An expression for the generated current can be derived by imagining two charges $-Q$ and $+Q$ that move apart a distance x in an electric field E applied between two parallel plates. The potential between the plates separated by distance l is

$$V = El. \tag{2.6}$$

The work required to move the charges a distance x in the electric field is

$$W = QxE = Qx\frac{V}{l}. \tag{2.7}$$

Work is also related to the current I running in the external circuit by

$$W = VIt, \tag{2.8}$$

where t is the time during which charges are collected. Solving I and inserting Equation 2.7 gives an expression for the current generated by the traversing radiation.[14]

$$I = \frac{W}{Vt} = \frac{Qx\frac{V}{l}}{Vt} = Q\frac{x}{lt} \tag{2.9}$$

Expressing this with the drift velocity v gives

$$I = Q\frac{v}{l} = q_{\mathrm{gen}} l \frac{v}{l}. \tag{2.10}$$

In the final step the generated charge Q has been expressed with the number of electron-hole pairs created per unit length q_{gen} ($Q = q_{\mathrm{gen}} l$).[15,17] Alternatively, the equation can be derived using Green's theorem and Gauss' law, as has been done in reference [21]. The number of generated charges is proportional to the deposited energy, hence measurement of the generated current can be used to determine the particle energy when it stops within the detector. Accurate and reliable determination of the deposited energy requires full collection of both electrons and holes.[14–16]

But not all charges reach the electrodes. Some carriers might be trapped for a certain time period within the crystal, or recombine with charges of opposite sign. Recombination removes charges from the signal lowering the measured energy deposition of each event. The time it takes on average until charge carriers recombine and disappear is called charge carrier lifetime. If trapped charges are accumulated in the detector bulk the device can suffer from polarization. Accumulation of charges in the interface between the detector bulk and metal contacts can also lead to polarization.[2,13,16,19,23] Polarization leads to reduced resistance and finally detector breakdown. Also, the electric field is no longer homogeneous because the accumulated charges create their own electric field in a direction opposite to the applied electric field. Accumulation of charges causes first a gradual decrease and then an abrupt drop in signal amplitude, charge collection efficiency, count rate and charge carrier velocity during detector operation. Polarization can be removed or reduced by switching the polarity of the bias voltage, switching the bias off and on again, by warming the crystal, or by irradiation with light of suitable wavelength. However, studies on irradiated samples have shown that these methods are not enough in samples irradiated with high fluxes. These samples require other methods, such as filling of traps (priming) and reprocessing, to fully counter effects of polarization.[2,15,20,23] Traps can be filled by low flux irradiation. Traps are filled with electrons produced by the radiation and passivated. The device can remain passivated for months if kept in dark and the traps are deep within the band gap. Exposure to light will release the trapped charges and depassivate the detector.[5]

2.3 Radiation damage

Semiconductor crystals always contain defects and impurities originating from the detector manufacturing and crystal growth. These defects are discussed in Chapter 4. In addition, there might be defects caused by radiation damage. Radiation detectors will suffer from radiation damage after some time, especially in high

radiation environments. Proper operation of semiconductor detectors is based on nearly perfect crystal structures with no defects. Radiation damage changes the crystal structure of semiconductors by formation of defects, which can lead to changes in the electrical properties of the material.[13] The effects of impurities and defects in the crystal structure are discussed in more detail in Section 4.1. Generally, radiation damage has a negative effect on semiconductor properties and leads to degraded detector performance and shortened lifetime.[16] In low radiation environments these effects are usually small, but in high radiation conditions the changes can be significant. One way to increase radiation tolerance is to reduce the detector thickness. This shortens the charge collection distance and the distance the radiation interacts with the material. However, since the amount of charge generated by radiation is proportional to the detector thickness, reducing the device thickness will also affect its sensitivity.[1]

Interactions of ionizing radiation with the detector material can lead to both reversible and irreversible changes in the crystal structure. Energy transfer through ionization and formation of electron-hole pairs used in the detection is a reversible change, while non-ionizing energy transfer leads to irreversible changes.[15] These irreversible changes are commonly displacements of atoms from their lattice sites, which are called a Frenkel defects and lead to interstitial lattice atoms and neutral vacancies. Lattice atoms are displaced when the radiation scatters from the atom and gives it enough energy to break free from its bond. The defects produces additional energy levels that are generally deep within the band gap. These defects act as trapping and generation-recombination centers and affect charge carrier lifetimes and collection of both charge carrier types. The charge collection efficiency can be reduced even further by radiation damage in the interface between the detector bulk and the metal contacts.[1,2,12,15,24]

In semiconductor detectors radiation damage leads to increased leakage current. [24,25] The additional energy levels in the band gap reduce the energy charge carriers need to move between the valence and conduction band. This shortens the charge carrier generation lifetime and increases the charge flow between the bands. Defects that act as traps capture charges and reduce the charge collection efficiency.[12,25] This leads to shortening of carrier recombination lifetime and signal reduction.[25] Because of the increased leakage current and reduced charge collection efficiency, detectors suffering from radiation damage will have worse energy resolution than non-damaged radiation detectors.

Radiation damage can also be observed as a change in effective doping density.

Point defects produced by the radiation can form defect complexes with either positive or negative charge. These complexes are called effective donors and acceptors. Point defects can also remove original donors by binding them in defect complexes. Examples of this type of complexes are vacancy-boron and vacancy-phosphorous complexes in silicon. In worst cases, after long term radiation exposure, the change in effective doping density can in N-type semiconductor detectors leads to type inversion, which means that the N-type semiconductor becomes P-type. P-type detectors don't undergo type inversion and instead become increasingly P-type after long term radiation exposure[26].

3. Diamond radiation detectors

Diamond has unique properties, e.g. breakdown voltage, wide band gap, high charge carrier mobility and radiation hardness, that make diamond attractive for many applications in both science and technology. The high quality of single crystal diamond produced with chemical vapour deposition techniques leads to additional advantages for radiation detection applications, e.g. reduced polarization effects and smaller need for detector priming (i.e. filling of traps by e.g. irradiation, see Sections 2.2 and 4.1). The many unique properties of diamond make it seem like an ideal material. However, the use of diamond in some applications is limited by the wide band gap, and the small signal resulting from the larger energy required to form one electron hole pair.[5,15,17,27] But the main disadvantage of especially single crystal diamond is its high price.[4] Table 3.1 lists some properties of diamond and silicon that are important for detector applications.

Many of the unique properties of diamond are a result of the crystal structure and the way atoms are bound to each other. Diamond consists of sp^3-hybridized carbon atoms and each carbon atom is covalently bound to four other carbon atoms in a tetrahedral geometry.[13,14,28] Because carbon atoms are small they can come close to each other before experiencing repulsive forces from each other. This results in relatively short atomic bonds and tight packing of atoms, giving diamond its high density and low compressibility.[13–15,29] The strength of the bond between the atoms makes the lattice rigid and strong.[14,28] Combined with the high density, the rigidity and strength of the crystal make diamond stable, hard and wear resistant.[11,14,30] The stability allows operation of diamond detectors even in high temperatures under high magnetic fields and voltages.[27] The strength of the atomic bonds makes dislocation of the carbon atoms hard, which is why diamond is hard to scratch, and it usually won't break due to dislocation creep or crack propagation.[14,30] In dislocation creep a part of the crystal moves relative to the rest of the crystal. The movement occurs point by point along a plane.[31,32] Crack propagation is the growth of cracks due to external loading. There are three growth modes; opening, sliding and tearing. In opening mode the crack surfaces are moved apart from each other. In sliding the crack surfaces move parallel to the

Property	Diamond	Silicon
Atomic number	6	14
Density [g/cm^3]	3.5	2.33
Band gap [eV]	5.47	1.12
Resistivity [Ωcm]	$10^{13} - 10^{16}$	$2.3{\cdot}10^3$
Intrinsic carrier density [cm^{-3}]	$< 10^3$	$1.5{\cdot}10^{10}$
Breakdown field [V/cm]	10^7	$3{\cdot}10^5$
Electron mobility [cm^2/(Vs)]	1800–2200	1500
Hole mobility [cm^2/(Vs)]	1200–1600	500
Saturation velocity [cm/s]	$2.20{\cdot}10^7$	$1.00{\cdot}10^7$
Dielectric constant	5.7	11.9
Electron-hole pair creation energy [eV]	13	3.6
Displacement energy [eV/atom]	43	13–20
Thermal conductivity [W/(cmK)]	20–24	1.5

Table 3.1: Properties of diamond and silicon.[12,14,16–18,25,27,30]

crack direction, while in tear mode the surfaces move perpendicular to the crack direction.[32]

The structure of the crystal gives diamond a large band gap of 5.47 eV. The size of the band gap makes diamond an insulator, but because diamond has many similarities with conventional semiconductor materials it is often categorized as a semiconductor.[12,14,15,17,23] Electrical properties of semiconductors are mainly determined by the band gap.[14] Important properties resulting from the large band gap are the low intrinsic carrier density and the low leakage current. The large band gap combined with the bond strength makes thermal excitation of charge carriers to the conduction band unlikely. Because leakage current is proportional to the intrinsic carrier density, diamond detectors have smaller leakage current than corresponding detectors made of other semiconductor materials. At room temperature leakage current of natural diamond is usually less than 10^{-12} A for voltages up to several hundred volts.[11,12,15,17,23] This leads to low power consumption and hence low energy dissipation[4,17], and low noise even at room temperature[11,18,23]. Diamond is suited for detector applications at high temperatures and its use at temperatures of $400 - 600$ °C has been reported.[33] The band gap energy corresponds to a wavelength of 225 nm, which is within the deep ultraviolet region. This makes diamond optically transparent for radiation ranging from the deeper half of deep ultraviolet region to far infrared and even radio frequencies. Because diamond is transparent to a wide range of wavelengths detectors often don't need windows to select a specific radiation type, or screening or packing to stop surrounding light. Solar-blind detectors for measurement of ultraviolet light take advantage of the improved discrimination between ultraviolet

light above the band gap energy and visible light.[4,15,16,18,28,29] A disadvantage followed by the large band gap is that the energy required to produce one electron-hole pair is quite large compared to other semiconductor materials. Because the energy required to form one electron-hole pair is larger, the number of charge carriers, and hence also the signal, is smaller in diamond than in many other semiconductor materials. The signal is further reduced by charge trapping.[5,17,18,34]

Diamond has high charge carrier mobilities and saturation drift velocities.[17,23] The saturation drift velocity is about $2.2 \cdot 10^7$ cm/s, which is a factor of 2 higher than in silicon.[12,15,23,28] The mobilities can be very different depending on the crystal quality and diamond type, but typical values are $1800 - 2200\,\mathrm{cm}^2/(\mathrm{Vs})$ for electrons and $1200 - 1600\,\mathrm{cm}^2/(\mathrm{Vs})$ for holes.[14,18] High mobilities and drift velocities lead to fast charge collection and short response times. Also, because electrons and holes have similar mobility they are collected at almost the same time.[11,14,15,23,34] These lead to less signal pileup and summation of events.[18] In many semiconductor materials, e.g. silicon, breakdown happens before the saturation drift velocity is reached. But with diamond the saturation drift velocity can be reached. This is due to the high breakdown electric field, which can be up to 10^7 V/cm, more than one order of magnitude higher than in silicon. The high breakdown field also allows operation of diamond detectors over a fairly wide voltage range.[12,25,28] The fast signals and high breakdown electric field make it possible to design systems for high speed and count rate measurements.[17,18] Diamond also has a smaller dielectric constant compared to many other semiconductor materials. The detector capacitance is determined by the dielectric constant and the device geometry. The capacitance in turn affects the noise level of the readout. Thanks to the smaller dielectric constant and lower capacitance, diamond detectors have less noise than silicon detectors of corresponding geometry.[5,15,23,25,34] The product of the input resistance of the circuit and the combined capacitance of the detector and the measurement circuit determines the time constant of the output signal. A small time constant produces fast signals, which is important in high event rates and when timing information is important. Low capacitance is therefore an important factor in timing applications.[4,11]

Diamond detectors can be used to detect any radiation with energy higher than the band gap energy, but the sensitivity of the detector strongly depends on the measured radiation type and energy[1,18]. The small atomic number of carbon reduces multiple scattering, which is preferred in tracking where particles should travel in near straight line for accurate position determination, but it also

makes measurement of highly penetrating radiation, such as high energy gamma radiation, difficult. The small atomic size makes the interaction cross section for highly penetrating radiation small, which reduces the detection efficiency. The sensitivity is reduced further by the high energy required to form one electron-hole pair. Thanks to the tight diamond lattice there are many atoms to interact with, but the higher density is not able to fully compensate for the smaller cross section and large energy required to form one electron-hole pair. Therefore diamond detectors are not that well suited for measurements of very penetrating radiation.[13,18,34]

Diamond has high thermal conductivity.[5,14,17,28,30] This property allows operation of diamond detectors in environments where the active cooling of the detector is not practically achievable or impossible.[5,15,17] Diamond has an unique combination of high thermal conductivity and low electrical conductivity, which is a rare combination in nature. This combination is explained by the heat transport mechanism.[13,14] In many semiconductor materials heat is mainly transported by electrons, hence high thermal conductivity comes with high electrical conductivity. However, in diamond the heat is mainly transported by lattice vibrations because there are very few free charge carriers that can transport heat due to the large band gap.[14,15,28,30] But because heat is mainly transported by phonons, thermal conductivity of diamond is more sensitive to crystal defects and crystal quality. Defects lead to increased phonon scattering and reduced thermal conductivity.[30] High thermal conduction is important in cooling applications. Electronics often require transportation of heat away from a small region it is produced at. The fast heat transportation makes diamond well suited for electronics cooling, especially in particle colliders due to its radiation hardness. In addition, diamond itself will not produce much heat due to the its high resistivity.[14]

Thanks to the strength of the atomic bonds and rigidity of the lattice, diamond is more resistant to radiation damage than many other semiconductor materials.[11,12,14,23,35] Radiation damage leads to atom dislocations and other crystal defects, which requires relatively high energy in diamond.[23] The energy required to permanently displace an atom from the lattice is around $43\,\mathrm{eV}$ in diamond and $13 - 20\,\mathrm{eV}$ in silicon.[17,28] Thanks to the relatively high binding energy of carbon atoms in the diamond lattice, the number of atom dislocations in diamond is smaller than in other detector materials exposed to the same amount of irradiation.[12,15] Radiation damage won't affect the leakage current of diamond as much as in e.g. silicon, due to the large band gap and naturally low leakage current of diamond, but formed traps affect carrier drift and signal size.[24] The radiation hardness makes it possible

to operate diamond detectors in high radiation environments.[18,25], which is why they are well suited for tracking in high energy physics.[11]

Another field for which diamond is an attractive detector material is medicine. The atomic number of diamond ($Z = 6$) is similar to the effective atomic number of human soft tissue ($Z \approx 7.5$).[11,14,18] This makes diamond tissue equivalent, which simplifies dose calculations since the dose to tissue can be obtained directly. [18,36] Diamond and human tissue also have similar response to photon radiation.[29] Because diamond is chemically inert and non-toxic, devices made of diamond won't react with the body or have harmful effects in the patient.[14,36] The better resistance to radiation damage means that the detectors can be used for a longer period of time before they need to be replaced.[11] Other appreciated properties are the small size, good energy resolution and efficiency.[36]

3.1 Classification of diamond

There are different types and quality of natural diamond, which is why a classification system has been developed. The classification system is shown in Figure 3.1. It is good to know about this classification system since many earlier applications used natural diamond and older literature often refer to natural diamond.[14] Even though the classification system was developed for natural diamond, the system can also be applied to synthetic diamond. However, this simple classification system can not distinguish between different synthetic diamond types with tailored properties manufactured today.[28,37] The classification is based on the impurities present in diamond. Due to variations in both impurity types and and concentrations, different diamond types have different properties. For example electrical conductivity of type IIb diamond is 13 times larger than type I diamond.[14] Impurities and their effects on properties of diamond and other semiconductor materials are discussed in more detail in Chapter 4.

Nitrogen is the most common impurity in natural diamond and the concentration of nitrogen is the base of the classification system. Depending on the presence of nitrogen, diamond can be divided into type I and type II diamond. These two main types are further divided into subtypes according to the arrangement of the nitrogen impurities and the presence of boron, which is another common impurity in diamond. Natural diamond can also contain other impurity atoms, such as iron or nickel, but these are not included in the classification system.[37]

Diamond that contains nitrogen impurities is categorized as type I. The nitrogen

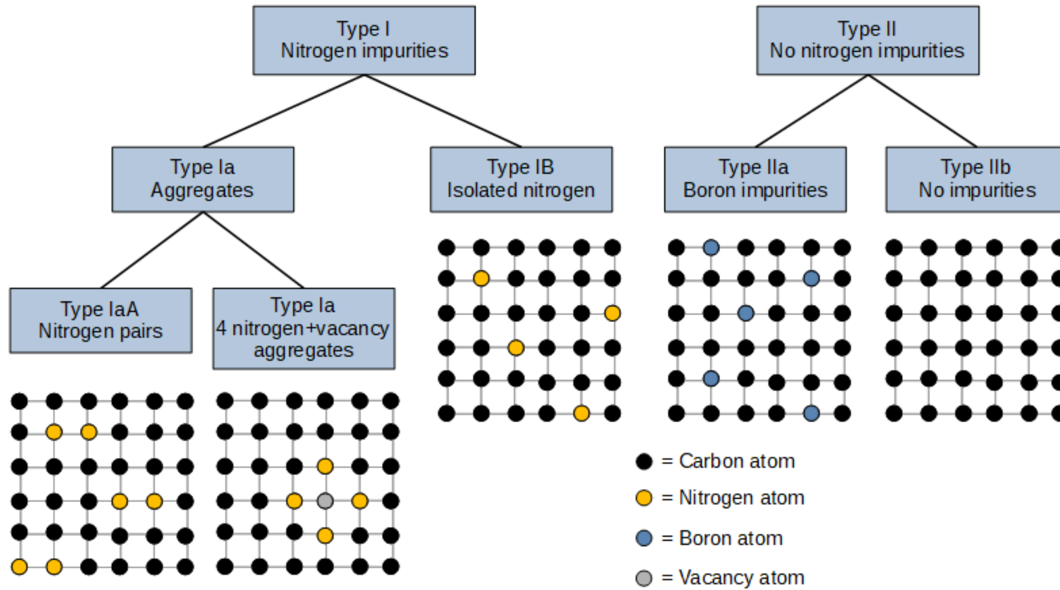

Figure 3.1: The classification system of natural diamond.

concentration is larger than 5 ppm, typically 100 − 3000 ppm. If the nitrogen is present as aggregates the diamond is type Ia, and if the nitrogen occurs as isolated atoms the diamond is type Ib. Type Ia is the most common diamond type in nature. Over 98 % of natural diamond is type Ia. Type Ia can be further divided into type IaA and type IaB.[28,37] In type A the aggregates are pairs of nitrogen atoms, while in type B the aggregates consist of four nitrogen atoms symmetrically organized around a vacancy. There are also other nitrogen aggregates, such as nitrogen-vacancy pairs, nitrogen-vacancy-nitrogen aggregates, and charged aggregates, but these are not included in the classification system. Figure 3.2 shows some examples of nitrogen aggregates present in diamond. Type I diamond is transparent to UV-light below about 300 nm, but due to the nitrogen impurities it strongly absorbs IR-light in some regions.[37]

Type II diamond does not contain nitrogen. In practice the diamond may not be completely free of nitrogen, the concentration is just so low that it can't be observed in IR absorption spectroscopy, typically less than 5 ppm. Type II diamond is rare in nature. Type II is subdivided into type IIa and type IIb based on the presence of boron. Type IIa is free of nitrogen and boron impurities. Synthetic diamonds produced by chemical vapour deposition are usually type IIa diamonds. In type IIb there are boron impurities but no nitrogen impurities. The increased electrical conductivity of type IIb diamond is due to the boron impurities. P-type diamond doped with boron falls within this category.[28,37]

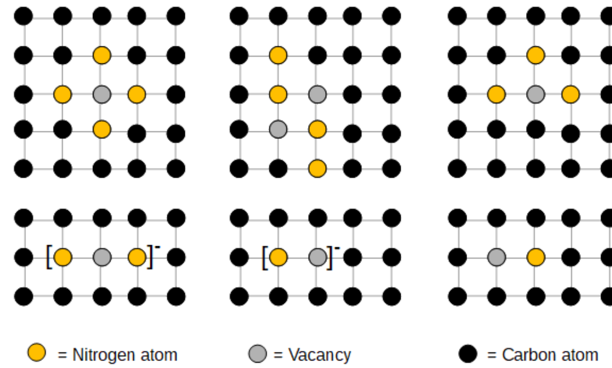

Figure 3.2: Examples of nitrogen aggregates present in diamond.

3.2 CVD diamond

The use of diamond in radiation detection applications was previously small due to the limitations of natural diamond. Natural diamond is expensive and and single crystal diamond is rarely found as large crystals. It often contains high concentrations of impurities and crystal defects that limit carrier lifetimes and charge collection. One disadvantage with natural diamond is the lack of control of material properties.[12,16,18,28,29] The wider use of diamond was made possible by development of production methods of artificial diamond. Synthesis of diamond has reduced the price of diamond and it allows better control of material properties. Artificial diamond can be produced in larger sizes with reproducible properties and lower concentration of impurities and crystal defects.[1,12,14,15,30,38]

Today artificial diamond is mainly produced by chemical vapour deposition (CVD) techniques. [28–30] CVD is a technique in which the crystal is slowly grown layer by layer as a result of chemical reactions happening in the gas phase above a solid surface under controlled conditions.[14–16,39] The method requires activation of the gas phase with combustion flame (e.g. oxygen acetylene torch), thermal methods (e.g. hot filament) or electric discharge (e.g. microwaves).[15,17] There are different CVD techniques with different parameter values and details, but they all have some similarities e.g. the substrate is heated to temperatures above 700 °C to guarantee formation of diamond instead of amorphous carbon, and most use a methane-hydrogen gas mixture.[15,29,39] The used gas mixture, temperature and pressure determine the number of defects, and therefore the properties of the CVD diamond.[13] Special care must be taken during the growth to not include nitrogen impurities, since they have been proven to have a negative effect on detector properties.[35]

In the synthesis process the substrate and the gases are placed inside a chamber,

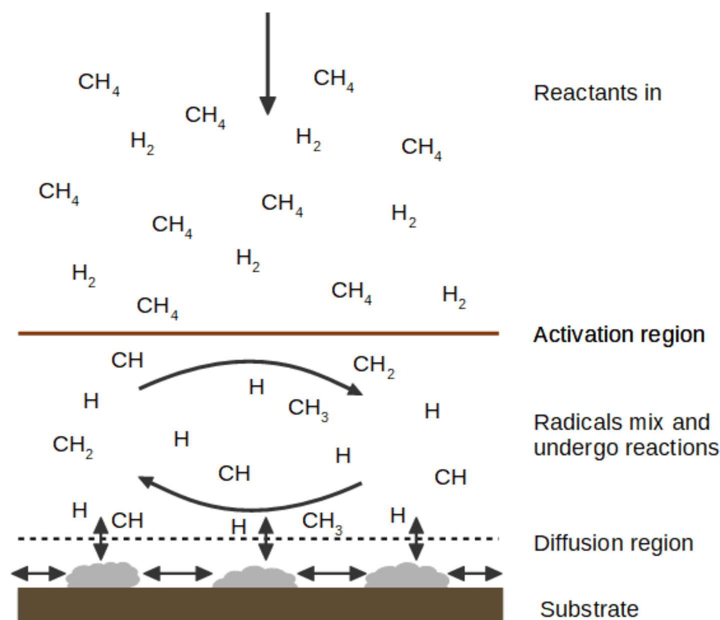

Figure 3.3: The chemical and physical processes in production of CVD diamond.

where the gas is mixed, see Figure 3.3. The gas diffuses towards the substrate surface. As the gas diffuses downwards, it passes the activation region where the gas is heated up to a few thousand kelvin, and the molecules are provided with additional energy by e.g. a hot filament, laser, direct current or microwaves.[14–16,29] The additional energy excites the molecules and breaks them into ions and electrons, leading to formation of reactive radicals and atoms that continue to diffuse towards the substrate. The species mix and undergo chemical reactions until they reach the substrate surface, where several processes can happen. The species can be absorbed and react with the surface, they can be desorbed back to the gas phase, or they can diffuse on the surface until they hit a suitable reaction site.[29] If the processing conditions are right, the reactions lead to formation of diamond.[14,15,29]

The gas is a mixture of carbon compounds hydrogen and oxygen. Commonly the gas mixture consists of methane and hydrogen, in which the methane fraction is typically $1 - 15\,\%$. The carbon compounds supply the process with carbon atoms in form of radicals that nucleate when they come in contact with the substrate.[15,16,29] Hydrogen has several important roles in the gas phase. Hydrogen undergoes thermal dissociation and forms reactive radicals when it reacts with neutral species in the gas mixture. It terminates dangling bonds of carbon atoms close to the surface, and it breaks long hydrocarbon chains preventing formation of large rings and polymers in the gas phase. Hydrogen also reduces the formation of graphite, since it is more effective at etching graphite than diamond.[15,16,29,39] Dopants are usually added

in the gas phase if they are needed.[16]

Diamond can be grown on different substrate materials, e.g. silicon, molybdenum or diamond, but the material has be able to withstand the processing conditions. The melting point at the processing pressure should be higher than the temperature the diamond is grown at. The substrate temperature depends on the technique, but it is between 770 K and 1470 K.[29,39] The substrate material and diamond should have similar thermal expansion coefficients. The substrate expands with rising temperature onto which the diamond is then grown. When the temperature is decreased both the substrate and diamond contract. If the expansion coefficients are different and the substrate contracts more, the diamond will experience significant compressive stress. This causes bowing and can result in cracking, flaking and in worst cases delamination of the film from the surface. If the goal is to produce an adherent film, i.e. a film that is attached to the surface, the substrate should be a material that can form a carbide layer. The interstitial carbide layer works like glue and binds the diamond to the substrate. In case one wants to form a free-standing diamond film one should chose a substrate material that does not form a carbide layer.[29]

3.3 Polycrystalline and single crystal diamond

CVD techniques can be used to grow both polycrystalline and single crystal diamond. Single crystal diamond consists of only one crystal. It is formed when the diamond is grown on a single crystal diamond substrate. Polycrystalline diamond on the other hand consists of many single crystals bound together by a disoriented interface and it is typically formed when the substrate is non-diamond.[24,28,30] Because of the grain boundaries polycrystalline diamond has some disadvantages compared to single crystal diamond. The boundaries are also the reason why the use of polycrystalline diamond is limited in some applications.[20] Because of its better crystal quality, detector applications usually use single crystal diamond.[27]

The growth of polycrystalline diamond starts from many randomly positioned and oriented crystal seeds. The crystal grains grow in all directions until they meet another crystal. When the grains don't have room to grow to the sides they only grow upward from the surface. Larger crystal grains grow faster and tend to outgrow small crystals.[24,28,29] This leads to a columnar structure with grain sizes that increase with distance from the substrate. The larger grain size comes with reduced number of defects and grain boundaries, which results in improved crystal quality.[28,29,38]

Because of the change in crystal quality, charge collection distance and electrical properties of polycrystalline diamond vary with the distance from the substrate. The crystal quality is improved by growing thicker polycrystalline diamond that is thinned from the bottom by lapping to remove layers with poor crystal quality.[13,34]

Grain boundaries are the main source of leakage current in polycrystalline diamond. In single crystal diamond the leakage current is mainly due to point and line defects. For single crystal diamond the leakage current increases linearly with applied voltage, but for polycrystalline diamond the change is non-linear due to additional energy levels produced by grain boundaries.[27] Grain boundaries challenge uniform and smooth charge collection by acting as trapping and recombination centers.[13,25] Because of trapping and recombination charge collection efficiency of polycrystalline diamond is only around 50 %. Single crystal diamond that has less defects and trapping centers typically has charge collection efficiency over 95 % and charge collection distance close to the detector thickness.[24,30] Boundaries can also accumulate charges, which leads to formation of polarization fields that are superimposed on the applied drift field.[25,27] All these processes remove charges from the signals and change the energy deposition of each event, which leads to lower pulse heights, or even disappearance of some characteristic peaks from the spectra.[27]

3.4 Structure of diamond detectors

Thanks to its high resistivity diamond doesn't need doping or reversed biased pn-junctions to reduce leakage current.[13,15,16,18] This makes fabrication of diamond detectors easier than fabrication of silicon detectors.[15] But processing is not trivial due to the hardness of diamond.[28] The processing starts with lapping and cutting of the diamond to size and thickness suitable for the application.[38] Next the surface is polished in order to create a smooth surface for the metallization. The polishing technique should be selected correctly, since some techniques can lead to surface damage that affect the detector operation down to depths of a few µm.[7,17,18] Processing after the growth produces surface contamination, such as graphite phases, and smoothing of the surface leads to hydrogen termination of the diamond surface. These both lead to increased surface leakage current. Radiation detectors need an insulating surface, which can be achieved by oxygen termination of the surface.[15] Therefore removal of the contaminants and oxidization of the surface are important parts of the processing. These are achieved by wet chemical cleaning protocol

that involves e.g. cleaning with different acids and organic solvents.[14,15] Diamond detectors typically have metal-semiconductor-metal structure, in which the diamond, usually intrinsic CVD diamond, is sandwiched between two metal electrodes, see Figure 3.4. The metallic contacts are added to allow collection of charges from the surface with the help of an electric field, and to avoid accumulation of charges on the surface. Similar structures made of other semiconductor materials, such as silicon, require doping in order to reduce leakage current, which is not needed with diamond thanks to its high resistivity and naturally low leakage current.[11,14,18,34,35]

Figure 3.4: Structure of diamond radiation detectors (not to scale).

The metallic contacts can be either ohmic or Schottky (rectifying) contacts. In an ohmic contact, the contact resistance is small compared to the semiconductor bulk resistance. In a Schottky contact, the difference in the Fermi levels of the metal and the semiconductor forms a potential barrier that restricts the flow of charges. Schottky contacts conduct well with one polarity and poorly with the other. Ohmic contacts on the other hand conduct the same with both voltage polarities. Due to the inertness and wide band gap, there are not many techniques and metals available that can form good ohmic contacts with diamond. The production of good ohmic contacts can be challenging. Bad contacts result often in Schottky barriers and increase polarization effects.[4,15] Most materials form Schottky contacts on clean diamond surfaces.[40] The size of the Shottky barrier depends on the termination of the diamond surface. Studies have shown that the barrier is the smallest for clean diamond surfaces and the largest for oxygen terminated surfaces. Hydrogen termination of the surface will lead to a barrier between these two. From this one can conclude that cleaning and termination of the surface has a significant effect on the Schottky barrier height.[41]

Ohmic contacts are usually obtained by modifying the diamond surface in some way. The surface can be modified by e.g. sputtering with argon, or formation of a carbide layer between the diamond and the metal. Argon sputtering damages the surface and leads to formation of amorphous carbon and graphite. Deposition of e.g. gold on the damaged surface will produce an ohmic contact. However, annealing

makes these contacts rectifying. Commonly ohmic contacts are obtained by forming a carbide layer between the metal and the diamond. As previously mentioned most materials form rectifying contacts with diamond. However, some materials, such as titanium, chromium, molybdenum and tantalium, form carbides upon annealing.[40] Carbide forming metals are the best way to produce ohmic contacts on diamond.[4] The carbide layer reduces the contact resistivity and allows the formation of an ohmic contact. To be noted is that the carbide layer is not necessarily complete, but instead in patches.[33,41] It is believed that the carbide layer prevents the contact from becoming rectifying again.[40]

Previously, when the techniques were less developed, metallization was challenged by the hardness and chemical inertness of diamond.[16] Today, metals are added by sputtering or evaporation.[14,15,17,38] Contacts need to be designed so that charges can easily flow out from the diamond bulk, but the flow from the metal to the diamond is stopped.[15] The exact requirements for the metallic contacts depends on the application, but most application require stability at elevated temperatures and good adhesion, i.e. the metal should be well attached to the surface. Good adhesion requires a reaction between the diamond and the metal, which explains why metallization of diamond can be challenging. Good attachment is usually achieved by depositing a thin adhesion layer beneath the thicker contact metal layer.[41] The material for the adhesion layer should be a carbide forming metal, common choices are chromium and titanium. A thicker interconnect metal layer is deposited on top of the adhesion layer. The interconnect layer is made of a stable and inert metal, e.g. gold, and allows good contact with the electrodes and protects the underlying layers from oxidation.[4,14,17,28,38,41] Studies on Ti/Au contacts have shown that titanium can diffuse into the gold layer, reducing the quality of the contact. Mixing of the two layers can be stopped by depositing a thin barrier layer between the gold and the titanium. The barrier material should have slow diffusion in gold or non-reactive to oxygen, or both. A common material choice for the barrier is platinum, because it diffuses slowly in gold and does not easily form oxides.[33]

The samples in this study have contacts made of a 10 w% titanium and 90 w% tungsten alloy. The contact on the top consists of a pad that covers most of the diamond surface, and four strips. The bottom contacts consists only of the metal pad. The diamonds are etched and polished before deposition of the alloy by sputtering. 100 nm thick layers are deposited on both sides. After deposition the samples are annealed at 700 °C for 4 minutes to form an ohmic contact. There are two options for the deposition of the metal, shadow masking and lithography. With shadow masking

the edges of the metallized area are not as clear as with lithography and aligning the pads can be challenging. However, using a mask makes the processing faster since 20 samples, instead of only one, can be processed at once. For the studied samples the pad is done by shadow masking and the strips by lithography. Figure 3.5 shows the processed detectors glued and wirebonded to the readout board.

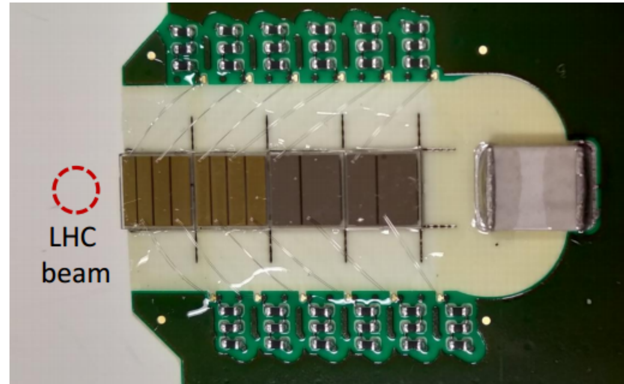

Figure 3.5: Diamond detectors glued and wirebonded to the readout board. Image source [8].

4. Defects

Ideal crystals have a continuous periodic structure and contain no foreign atoms or lattice irregularities. There are no perfect crystals in nature. Natural crystals always contain impurities or lattice defects. Because atoms are relatively immobile in solids, defects are hard to remove once they have been formed. Depending on their concentration defects can have a significant effect on semiconductor properties. The impurity concentration tend to determine electrical properties of semiconductors. This is why characterization of defects and knowledge of their effects is important.[11, 19,31,32,42]

Crystal defects are classified according to their dimensions. Zero dimensional defects are isolated errors in the crystal that are called point defects. One dimensional defects are lines that break the crystal periodicity and are called dislocations. Two dimensional defects are surfaces and are called interfacial defects. In three dimensional defects the crystal irregularity extends over some volume. These are called volume or bulk defects.[31,32]

Point defects can be vacancies, impurities or self-interstitials, see Figure 4.1. Vacancies are empty sites in the crystal lattice that should contain atoms. These are always present in crystals.[31,32] Vacancies govern diffusion of atoms in solids, since easy migration of atoms requires that atoms move to positions that are free of other atoms.[31] When the defect is an atom placed in a position that normally is free the defect is called a self-interstitial. Atoms are larger than the free space between the atoms so self-interstitials cause large distortions in the crystal. This is also why self-interstitials are not as common as vacancies. Impurities are foreign atoms that are intentionally or unintentionally added into the crystal. Impurities can substitute lattice atoms or be placed in interstitial positions.[31,32] Substitution is more likely when the impurity atom and lattice atoms have similar size. Interstitial atoms on the other hand must be small due to the limited space between lattice atoms. In order not to alter the crystal too much interstitial atoms must be smaller than the host atoms.[31,32,43] Intentional addition of impurities is called doping and it is used to modify some material property, e.g. corrosion resistance, electrical conductivity, or mechanical property.[31,32]

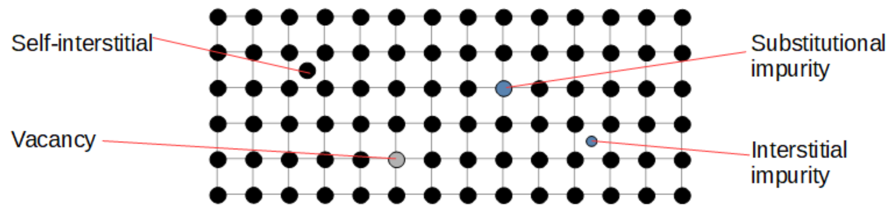

Figure 4.1: Point defects

Linear defects, or dislocations, are misalignments that break the periodicity of the crystal. These can be screw dislocations, edge dislocations or mixed dislocations. Edge and screw dislocations are illustrated in Figure 4.2. If a part of the crystal is shifted relative to other parts of the crystal, the defect is called a screw dislocation. Edge dislocations are defects in which a plane of atoms ends within the crystal. Mixed dislocations are a combination of screw and edge dislocations. These are the most common linear defects.[31,32] Dislocations are always present in crystals and they can be formed e.g. during crystal growth, during deformation, or due to thermal stress.[32] Dislocations are generally unwanted in semiconductor applications since they have a negative effect on electrical properties.[31]

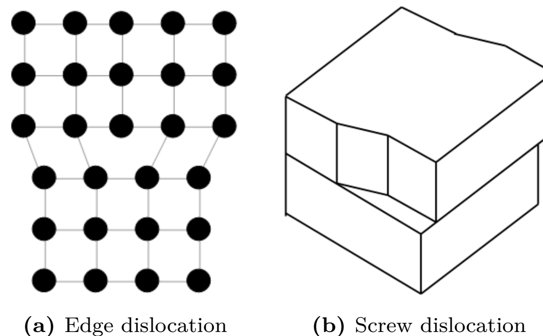

(a) Edge dislocation **(b)** Screw dislocation

Figure 4.2: Examples of linear defects in crystals.

Interfacial defects are two dimensional boundaries.[31,32] There are three types of surface defects, free surfaces, intercrystalline boundaries and internal defects. Figure 4.3 shows a free surface, a boundary and two types of internal defects. Free surfaces are external surfaces that terminate the crystal and determine the shape of the crystal. Intercrystalline boundaries interrupt the periodicity of the crystal and separate crystal grains that can also have different composition or crystal structure. Free surfaces and intercrystalline boundaries both contain atoms that are not bounded to the maximum number of neighbours.[31,32] The atoms with dangling bonds want to get rid of the asymmetry and are favorable locations for adsorption of foreign atoms from the surrounding.[31] Atoms at the boundaries are

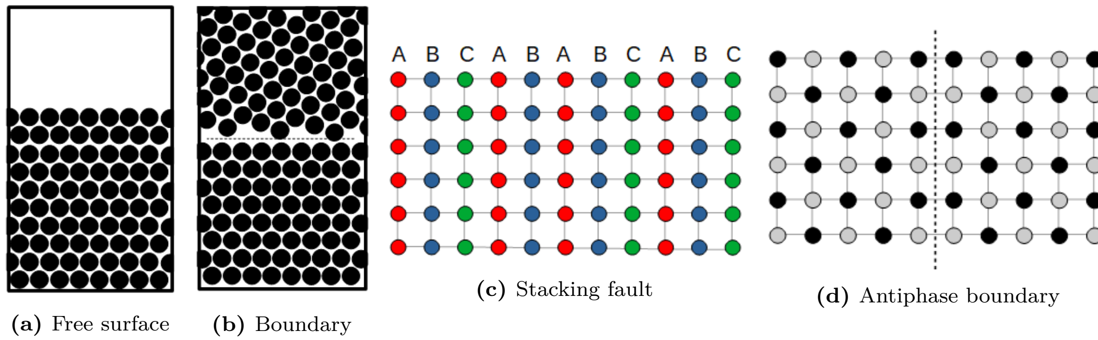

(a) Free surface (b) Boundary (c) Stacking fault (d) Antiphase boundary

Figure 4.3: Examples of interfacial defects in crystals.

irregularly bonded and both bond length and angle vary.[32] Two common types of internal defects are stacking faults and antiphase boundaries. Stacking faults are errors in the stacking of close-packed planes. Antiphase boundaries are only present in ordered compounds.[31]

Volume defects are larger than the defects described so far.[32] These are three dimensional aggregates of vacancies and atoms. There are four types of volume defects. Precipitates are very small volumes, with different crystal structure. These are typically a fraction of one µm in size. Dispersants are second-phase particles that can have very different sizes, from a fraction of 1 µm to up to 100 µm. Inclusions are dirt that have entered the crystal during its growth or precipitated atoms. These come in different sizes, from a few µm to macroscopic size, and are quite large. Inclusions are unwanted in most applications. Voids, or pores, are formed either when vacancies accumulated at one place or by trapped gasses. Voids are also generally unwanted defects e.g. because they decrease the mechanical strength of the material.[31] Volume defects can also be cracks, other phases or other larger crystal deformations.[32] Volume and lower dimension defects reduce the mechanical strength of the material and can make device manufacturing challenging. Defects can e.g. affect the diffusion of dopants, work as impurity sinks or generation sites for linear defects. Inclusions and precipitates can also alter the electrical properties of the material.[31]

4.1 Effect on semiconductor properties

Usually, defects don't significantly change essential properties of materials, such as melting point and the elastic modulus. But electrical properties, such as conductivity, charge carrier mobility and charge carrier lifetime, are significantly affected by variations in the crystal structure.[10,42] Whether the change in the property is

wanted or not strongly depends on the application. For example short charge carrier lifetimes are wanted in switches but not in radiation detectors. Today structural defects and impurities are intentionally added to material in order to produce materials with desired properties. For example charge carrier lifetimes can be controlled by growing structurally perfect pure crystals and intentionally introducing lifetime shortening defects. It is important to study defects and their properties in order to be able to add defects with wanted properties and remove those with undesired properties.[42]

The change in electrical properties are due to defect energy levels. In perfect crystals there are no energy levels in the band gap and charge carriers need to move directly between the valence and conduction band. Defects alter the crystal structure and lead to formation of additional energy levels within the band gap. These energy levels allow charges to move between the valence and conduction band with energies less than the band gap energy, see Figure 2.2.[19,42] This impacts carrier densities and mobility, as well as carrier lifetimes and trapping probability.[10] How defects affect the electrical properties depends on the location of the energy levels within the band gap.[42]

Defects are divided into shallow and deep defects. Shallow defects are divided into acceptors and donors. The simplest definition is that shallow defects have energy levels close to the band gap edges, see Figure 4.4. The states are usually within a few tens of meV from the band edge. Deep defects mostly have energy levels deep inside the band gap, usually within the middle third.[11,42] But deep defects are also found that have energy levels close, or even inside, the conduction or valence band. A generally applicable definition is that deep defects have highly localized wave functions, while shallow defects have extended wave functions.[42] Wave functions of highly localized states overlap very little with the wave functions of the neighbouring states. The wave functions of extended states on the other hand overlap significantly with the neighbouring wave functions. Impurity atoms that fit well in the lattice have large overlapping of orbitals, and produce shallow energy levels. Badly fitting impurity atoms form deep levels because they cause large distortions in the lattice and have orbitals that overlap much less with the neighbouring orbitals. Conductivity requires significant overlapping of neighbouring orbitals. Therefore the concept of localized states explains why highly disordered crystals don't show conductivity.[42,44]

Deep defects have some properties that make them generally unwanted.[23] However, in some applications they are intentionally added to improve some property,

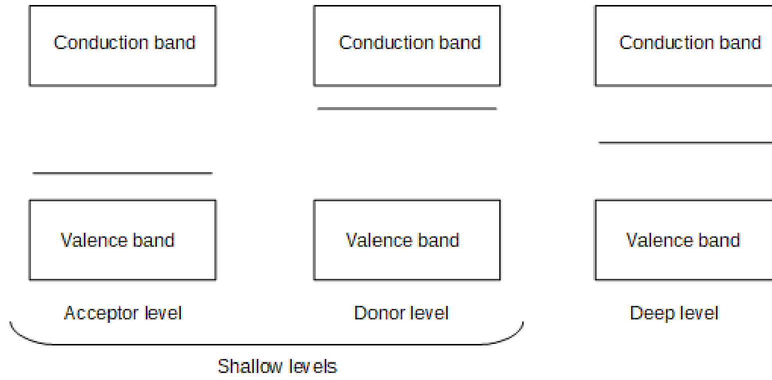

Figure 4.4: Simple definition of deep and shallow defects.

e.g. to shorten carrier lifetimes in switches.[19] Deep defects can act as traps or generation-recombination centers.[11,15,19] Whether a deep defect acts as a trap or generation-recombination center depends on many factors, e.g. temperature and capture cross sections, but a general rule is that defects in the middle of the band gap act as recombination-generation centers and those closer to the edges work as traps. Generation-recombination centers generate charges when the charge carrier density is less than the equilibrium value, and recombine charges when the carrier concentration exceeds the equilibrium density. [19]

Recombination centers first capture a charge from either the conduction or valence band, e.g. an electron from the conduction band. Next the center captures a charge carrier with opposite sign from the other band, e.g. an hole from the valence band, which leads to annihilation of the two charge carriers. Generation centers first emit an electron to the conduction band and then an hole to the valence band. The hole emission is followed by capture of an electron from the valence band. Traps capture charges from the energy bands and emit them after some time.[11,19] The longer distance the charges have to travel through the detector, the higher the probability that they are trapped before they are collected.[23] Both traps and recombination centers remove charges and contribute to signal reduction. Deep defects reduce the distance charge carriers travel before they are trapped and are the most effective reducers of carrier lifetimes.[10,11,42] In detector applications deep defects are highly unwanted since they lower detector performance by shortening carrier lifetimes and drift distances, and by removing charges before they are collected.[11]

Shallow defects are often used to control the type and charge of charge carriers in semiconductors.[11] This changes the electrical properties of the material and is achieved by intentional addition of impurities into the crystal in a process called doping. Doping can change semiconductor properties by several orders of

magnitude.[10,31,42] Impurities can be added into the crystal during crystal growth or later during processing. Ideally dopants are substituted into the crystal without changing the chemical bonds nor distorting the lattice.[10] This is easier to achieve with impurities that have similar size as the host atoms.[43] Addition of atoms with fewer valence atoms than the host atom leads to incomplete bonding and holes. By exchanging with holes electrons can move from bond to bond across the lattice. This process is called conduction by holes. Dopants that accept electrons from the valence band and increase conduction by holes are called acceptors. Semiconductors with excess holes are P-type semiconductors. Addition of atoms with more valence electrons than the host atom leads to saturated bonding and forces electrons into excited states. The excited electrons are free to move in lattice. Dopants that donate electrons to the conduction band and increase conduction by electrons are called donors. Semiconductors with excess electrons are N-type semiconductors.[10,31,42]

Deep defects can to some degree compensate effects of shallow defects if they act as trapping centers. Shallow defects increase movement of charges between the energy bands, while deep trapping centers reduce the charge flow. Therefore formation deep defects e.g. by radiation damage, can be observed as decreased leakage current. But if the deep defect act as a recombination-generation center, it will increase the charge flow between the bands and have the same effect as the shallow defect.[15]

Impurities and irregularities in the crystal structure lead to reduced and unstable detector response. There are several reasons for this change. As mentioned in Section 2.2, charges can be trapped within the detector by defects. If charge carriers are captured by traps the detector response will slowly decrease during operation as the number of filled traps increases. In case the traps are deep inside the band gap, charges will accumulate within the detector and form an additional electric field that affects the charge carrier drift. In sufficiently high temperatures, the thermal energy can excite the charge carriers to the conduction band and release them from the traps. This leads to an increase in the signal amplitudes.[35] The signal instability caused by charge trapping can be countered by filling traps before the measurement e.g. by irradiation. When the measurement is started the traps are already filled and will not capture charges forming the signal, which will lead to better charge collection efficiency, higher signals and increased detector stability.[13,15,35] Studies on CVD diamond have shown that filling of traps before the measurement can increase the signal by $30 - 100\,\%$.[34]

4.2 Defects in diamond

Even synthetic diamond grown in very restricted environments contains defects. Just like defects in other semiconductor materials, these defects can have a significant effect on electrical properties of the diamond.[39] These can be e.g. crystal boundaries, vacancy clusters or dislocations, self-interstitials. Some polishing techniques can also lead to lifetime reducing surface defects. Due to the atomic density and rigidity of the lattice, there is very little room for foreign atoms in the diamond crystal. Still it is possible for impurities to substitute carbon atoms, or to take interstitial positions in the lattice.[15,30] Two common impurities are nitrogen and boron, but diamond can also contain e.g. silicon, phosphorus, nickel, iron or sulfur.[30,36,37] Boron and nitrogen both have size close to the size of carbon atoms, which is why they are easily incorporated into the diamond crystal. Nitrogen is a major impurity in diamond. Usually nitrogen substitutes carbon atoms and can be present either as individual atoms or as aggregates. Nitrogen acts as a trapping center, affecting e.g. charge carrier lifetimes and detector sensitivity, which is why the concentration of nitrogen should be kept as low as possible. However nitrogen is very difficult to remove from crystal growth and processing.[15,18,30,36] Sometimes small amounts of boron are added into the crystal to compensate some of the negative effects of nitrogen and to produce P-type diamond. Boron can also enter the crystal due to contamination during the processing. However, boron impurities are shallow defects and can have a negative effect on detector performance.[15,36]

Modification of diamond properties by doping isn't as flexible as for silicon. Doping of diamond is challenging mainly due to the low mobility of dopants. This hinders the use of diffusion doping techniques commonly used with silicon.[14] P-type diamond has been successfully obtained with boron doping by incorporating boron compounds in the gas phase during crystal growth. Doping with boron produces energy levels 0.37 eV above the valence band. N-type diamond, however, is a challenge.[14,28,39,43] Nitrogen is a N-type dopant, but it forms quite deep energy levels when it bonds with four carbon atoms. An option is to use phosphorus which doesn't form as deep energy levels as nitrogen. The energy levels of phosphorus and nitrogen dopants are 0.6 eV and 1.7 eV below the conduction band.[28,39,43] But incorporation of phosphorus is more difficult because it has a larger covalent radius than carbon. Since N-type doping hasn't been successful, diamond can not be used to build bipolar structures such as PN-junctions.[43] However, due to its naturally high resistivity, diamond doesn't need doping or PN-junctions in radiation detector applications.[14]

5. Characterization

For optimal operation of a semiconductor detector one should have knowledge of the generation of leakage current and the charge carrier transport mechanism in the detector material. Properties such as charge carrier velocities and lifetimes, effective space charge concentration (i.e. the concentration of excess charges accumulated in a specific region, e.g. concentration of ionized dopants in a PN-junction) and dielectric strength determine the safe operational region of the device, and how much of the charges generated by the traversing radiation is collected. Many of the important electrical properties depend on the defect concentration, therefore the measurements give an idea of the crystal quality of the sample. Characterization of electrical properties allows selection of operational conditions and a device geometry such that the charge carrier drift time is shorter than their lifetime.[15,45]

The characterization should be done at different stages of the detector fabrication, in order to detect problems at an early stage and to get an idea of what could have caused it. This work describes the characterization and quality assurance process of CVD diamond detectors. The process starts with visual inspection of the samples by optical and cross-polarized light microscopy, after which the samples are sent for pre-metallization. The next step is to check the quality of the coating by optical microscopy and to perform a leakage current and charge collection efficiency measurement. The same measurements are repeated in the final step, after the metallization of strips. The main focus of this thesis is on the charge collection distance measurement. The other measurements are described for completeness.

5.1 Visual inspection

The purpose of visual inspections is to check whether the crystal is good enough to proceed in the processing. In the first step an optical microscope is used to make sure that there are no large deformations on the sample surface or pieces missing in the corners. The microscope was also used to check that the sample dimensions are correct. The samples have a truncated pyramid shape, i.e. a shape where one

side of the sample is slightly smaller than the other, see Figure 5.1. The samples are 500 µm thick, and have an area of $4.5 \times 4.5\,\mathrm{mm}^2$. After the metallization optical microscopy was used to check the quality of the metallization (e.g. no delamination or bridges between strips) and to make sure that the metal pads are aligned and the dimensions of the metallized areas are correct. The metallized area is $4.2 \times 4.2\,\mathrm{mm}^2$, leaving an unmetallized area extending 150 µm from the sample edges as shown on the right in Figure 5.1. This unmetallized area prevents discharges through the edge and reduces surface leakage currents. Usually when performing this kind of visual inspections, samples that show the slightest indication of not working properly (e.g. chipped corners or rough edges) are removed from further processing. But in this quality assurance process it was decided to keep all samples except the really bad ones in the processing, and decide whether the diamond sample performs well enough after all measurements have been completed.

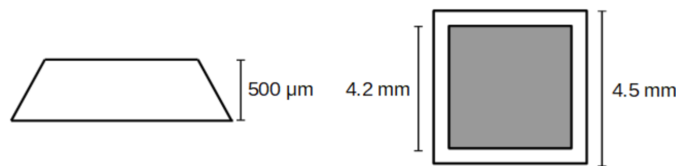

Figure 5.1: Dimensions of the diamond detectors (not to scale).

Figures 5.2 show examples of images from the optical microscope visual inspection before metallization. The different colour clearly visible in some of the images (e.g. Figures 5.2a and 5.2c) is due to the truncated pyramid shape of the samples. At the edges light passes through less material, which is why they are observed as slightly darker colour. The sample shown in Figure 5.2a has a clean surface since it has a clear colour. One of the edges is very straight and good, while the other is rough. Also, a piece has been cut off from the corner. The sample in Figure 5.2b

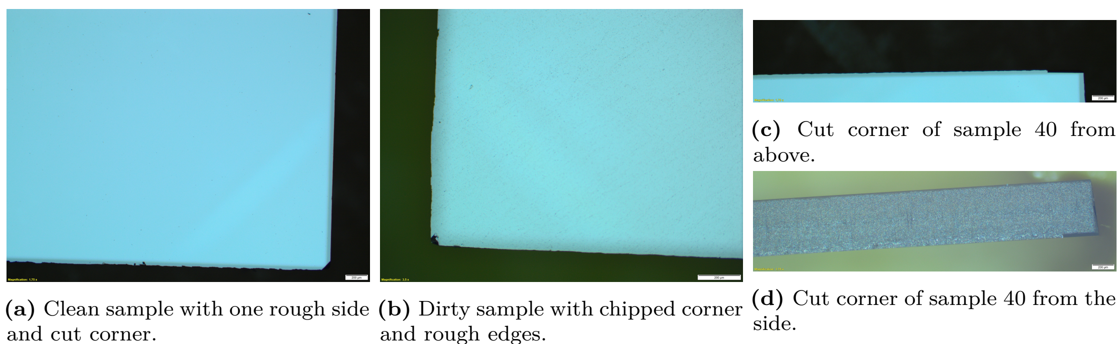

(a) Clean sample with one rough side and cut corner.

(b) Dirty sample with chipped corner and rough edges.

(c) Cut corner of sample 40 from above.

(d) Cut corner of sample 40 from the side.

Figure 5.2: Optical microscope images of diamond samples before metallization.

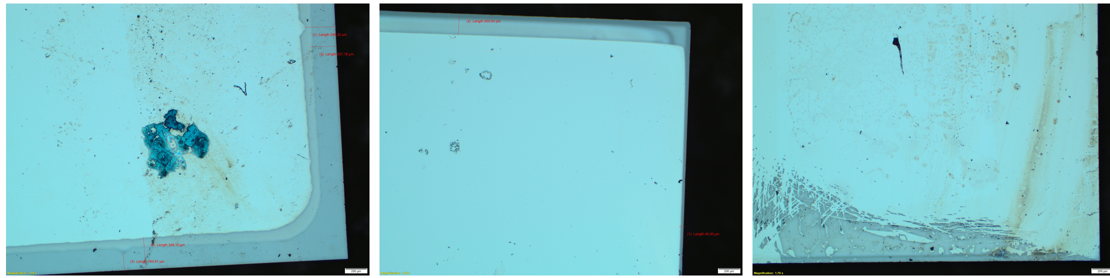

(a) Dirty sample with good metallization quality. (b) Sample with misaligned metallization too close to the edges. (c) Dirty sample with delamination of the metal.

Figure 5.3: Optical microscope images of diamond samples after first metallization.

is dirty and has a crack in the corner and rough edges. The dirt did not come off despite cleaning with isopropanol, which indicates that the surface is also rough. Sample number 40 had a piece cut off along one of the edges, which is an exceptional defect, see Figures 5.2c and 5.2d. None of the described defects are large enough to remove the sample from processing. The defects have to extend about 150 µm towards the sample centre for the sample to be unusable.

Figure 5.3 shows optical microscope images after the first metallization. The brown and dark areas on the surfaces are dirt from handling of the samples that did not come off in cleaning. Because diamond is transparent, one can see whether the pads on the top and the bottom are aligned or not. Figure 5.3a shows a sample with metallization of good quality. The pads are well aligned and not too close to the edge, and the pad edges are clear. Some deformations can be seen on the edges but they are so small that they won't affect detector operation. The other two images show examples of bad samples that need to be reprocessed. In Figure 5.3b the pads are misaligned and too close to the sample edges. Figure 5.3c shows a sample for which part of the pad has been torn off, indicating delamination of the metal.

The visual inspection before the metallization included an inspection with a cross polarized light microscope. Due to the symmetry of the cubic lattice, diamond is optically isotropic, meaning that the refractive index is the same in all directions. However, impurities and crystal defects can make the sample optically anisotropic.[15,28] These defects can be seen with cross polarized light microscopy. The sample is placed between two crossed polarizers. The first polarizer polarizes the light that passes through it and enters the sample. If the sample is isotropic, very little light will hit the recorder since the second polarizer blocks the initial polarized light. But in an anisotropic sample double-refraction causes the light to split to two components and a rotation in the polarization axis. Because the two light components have different optical paths, they exit the sample in different phases.

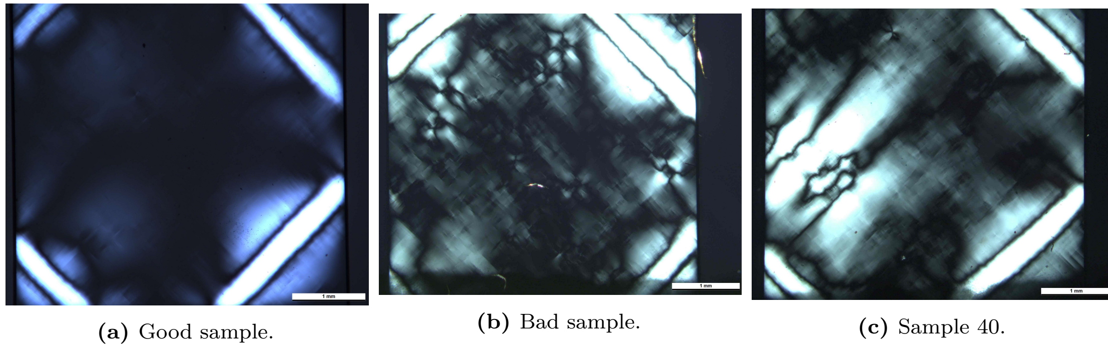

(a) Good sample. (b) Bad sample. (c) Sample 40.

Figure 5.4: Cross polarized light microscope images.

When the light hits the second polarizer some components can be parallel to the polarizer and pass through it. Regions where double-refraction occurs are seen as bright areas in the microscope image.[15]

Examples of images taken with the cross polarized light microscope are shown in Figure 5.4. The different colour of the images is due to different light settings. Defects and crystal irregularities are observed as bright lines and petal like shapes. The lines in the corners of the samples are due to tools used to handle the sample. Figure 5.4a shows a good sample with no bright areas except the lines at the corners. The sample in Figure 5.4b is categorized as a bad sample since it has many petals and some brighter areas. One of the lines in the corners is also missing. Figure 5.4c is the image taken of sample 40 with the exceptional defect in one corner. The image is very different from the images taken of other samples. No rejection limits have yet been determined for the cross polarized light microscope imaging because this is the first time the imaging is part of the quality assurance process. The limits will be determined after the electrical characterization, once the correlation between the observed defects and the electrical characteristics is known.

5.2 Leakage current

Leakage current is a property that is commonly used for electrical characterization of semiconductors.[27] In pure and defect free wide band gap semiconductors like diamond, thermal generation of charge carriers is negligible. However, impurities and irregularities in the crystal structure can introduce shallow intermediate energy level within the band gap that allow charges to move between the energy band with energies less than the band gap. A result of the reduction of the energy needed to move charges between the valence and conduction band is increased leakage current. [10,15,19,42] A current (I) over voltage (V) measurement can therefore provide

knowledge of the crystal quality and impurity concentration. The measurement can be used to determine the voltage region at which the detector can be safely operated without breakdown. Determination of leakage current also provides a rough estimate of the detector contribution to the noise level of the measurement system.[15]

5.2.1 Measurement of leakage current

The setup used for the IV-measurement is shown in Figure 5.5. The sample is placed in a radiofrequency shielded box on top of a vacuum chuck in a sample holder made of insulating plastic, together with a manipulator and a movable spring probe needle that is brought to contact with the top surface of the sample. The shielding box is a standard electronic cabinet made of steel, and it is used to reduce noise by protecting the measurement terminal and any exposed connections from electrostatic charges. The vacuum chuck, as well as the spring probe, are isolated from the bottom of the box. A magnet is used to attach the manipulator to a steel plate. The chuck-spring probe combination allows measurement of the sample without wirebonding it to a test board, hence simplifying the measurement and making it faster. The power is supplied to the sample by a Keithley 2410-C source meter unit, which is connected to the chuck with a safe high voltage (SHV) cable. The current is measured with a Keithley 6487 picoammeter connected to the spring probe with a triaxial cable. A Keysight 82357B USB/GPIB interface converter is used to connect both the picoammeter and the voltage supply to the measurement computer, where the data is collected using software based on MATLAB.

The measurement is performed by first decreasing the voltage in 50 V steps

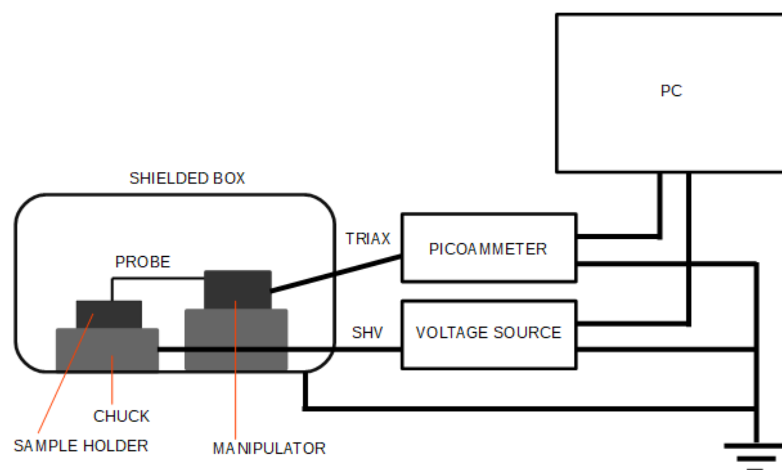

Figure 5.5: The setup for the leakage current measurement.

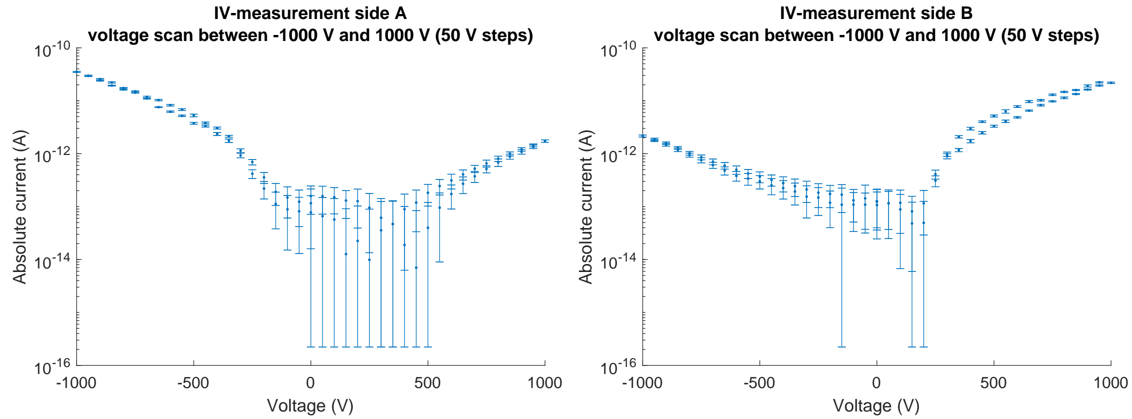

Figure 5.6: Results of the leakage current measurement for side A (left) and side B (right) on the reference sample.

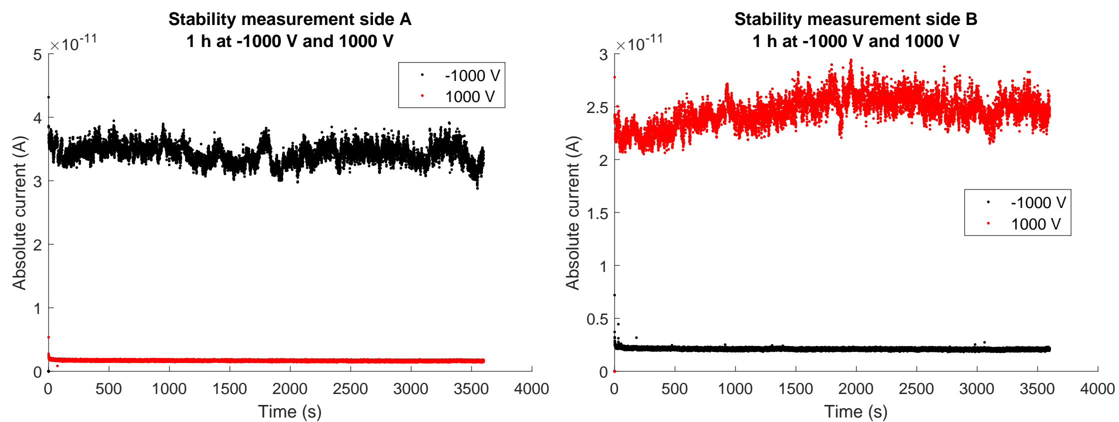

Figure 5.7: Results of the stability measurements for side A (left) and side B (right) on the reference sample.

from 0 V to −1000 V and afterwards increasing it in steps of 50 V back to 0 V. After this the voltage is first increased in same size steps to 1000 V, and then decreased back to 0 V. Each step is followed by a 5 min long stabilization period. When the system is stable the leakage current is measured for a suitable time period. The current is measured 60 times at each voltage in order to obtain a mean and standard deviation. The results are then visualized in an IV-plot. The stability of the detector is tested by measuring the leakage current at 1000 V and −1000 V for one hour. The length of the stability measurement can be reduced if necessary. Previous studies have shown that measurement times down to 10 min will produce representative results. Leakage current and its stability are measured on both metallized sides of the diamond detector. The strips are metallized on the side with lower leakage current.

Figure 5.6 shows the result of the leakage current measurement for both sides of a reference sample. Here the side on which the strips are metallized on is referred to as side B and the other side as side A. The bias voltage is applied from the bottom and the current is read from the top. The current increases as the voltage is ramped up and down from 0 V. The increase is faster and larger for one voltage polarity. For side A the leakage current is $(1.732 \pm 0.096) \cdot 10^{-12}$ V at 1000 V and $(-3.514 \pm 0.079) \cdot 10^{-11}$ V at -1000 V. Side B shows opposite behaviour, as expected. The leakage current is $(2.230 \pm 0.059) \cdot 10^{-11}$ V at 1000 V and is $(-2.156 \pm 0.095) \cdot 10^{-12}$ V at -1000 V. No signs of breakdown can be seen. Breakdown would be seen as a rapid increase in leakage current until picoammeter compliance of $1.05 \cdot 10^{-4}$ A is reached. Figure 5.7 shows the results of the stability measurements for the same reference sample. The leakage current is more stable for the voltage polarity with lower leakage current, i.e. for positive voltage on side A and for negative voltage on side B. In the quality assurance samples are rejected if the leakage current is not stable at ± 1000 V or if the current is larger than 10 pA at both voltage polarities. For samples with strips the leakage current and stability are measured for all strips. The same requirements have to be met for all strips as well as for samples without strips.

5.3 Charge collection distance and efficiency

Defects in the crystal structure act as trapping centers and remove charges from the signal. Charge collection distance, i.e. the average distance charge carriers move before they disappear, is a property that strongly depends on the crystal quality, which is why it is commonly used for material characterization.[13,16,17] In materials with large charge collection distance carriers are able to leave the material, which is why the carrier concentration will remain low and generated charges will not affect the electric field. A large charge collection distance is important in radiation detectors. When the charge collection distance is larger than the device thickness, all charges are collected at the electrodes. But if the charge collection distance is shorter than the device thickness, only a part of the generated charge will be collected. Uncollected charges can accumulate within the material and distort the applied electric field across the device.[11,14,15,18] Trapping can also lead to reduced charge collection, which in turn leads to shifts in the characteristic peaks to lower energies (lower signal amplitudes) and reduced resolution.[20]

The charge collection distance d is the mean distance electrons and holes move

apart before being trapped. It is a property that is strongly dependent on the charge carrier drift velocity v and lifetime τ.[15,17,24] It is the product of the mean carrier lifetime v_{avg} and the average drift velocity v_{avg}.[11]

$$d = \tau_{\mathrm{avg}} v_{\mathrm{avg}} \tag{5.1}$$

The charge collection distance is the sum of the mean distance electrons (d_{e}) and holes (d_{h}) travel.

$$d = d_{\mathrm{e}} + d_{\mathrm{h}} \tag{5.2}$$

In homogeneous electric fields, assuming the charge collection distance is smaller than the detector thickness, collection distance can be expressed using charge carrier mobilities (μ_{e} and μ_{h}).[15–17,38]

$$d = \tau_{\mathrm{e}} v_{\mathrm{e}} + \tau_{\mathrm{h}} v_{\mathrm{h}} = (\tau_{\mathrm{e}}\mu_{\mathrm{e}} + \tau_{\mathrm{h}}\mu_{\mathrm{h}})E \tag{5.3}$$

Because of charge carrier drift velocity v charge collection distance will depend on the applied electric field. Just like the drift velocity, charge collection distance increases linearly at low electric field strengths. At high fields the increase is non-linear until the charge collection distance saturates and reaches its maximum value.[17,34]

The charge collection distance is also described by the ratio of charge collected at the electrodes Q_{coll} to the charge generated by the radiation Q_{gen} multiplied by the detector thickness L. Charge collection distance for any thickness l can be expressed with the charge generated per unit length (q_{gen}).[13,14,17,38]

$$d = \frac{Q_{\mathrm{coll}}}{Q_{\mathrm{gen}}} L = \frac{Q_{\mathrm{coll}}}{q_{\mathrm{gen}}} \tag{5.4}$$

The generated charge is the mean number of electron-hole pairs one traversing particle produces. The generated charge is given by

$$Q_{\mathrm{gen}} = \frac{E_{\mathrm{p}} e}{\epsilon_{\mathrm{p}}}, \tag{5.5}$$

where E_{p} is the particle energy, ϵ_{p} the average energy required to produce one electron hole pair, and e the elementary charge.[20] A rough estimate of ϵ_p is about three times the band gap energy.[18]

Charge collection efficiency (CCE) is the ratio of collected charge to the generated charge. Charge collection efficiency tells how much of the generated charge is collected at the electrodes. It is a property that is often used to compare detectors.

In uniform electric fields the efficiency is assumed to be proportional to the mean charge collection distance. The following equation applies when the charge collection distance is smaller than the detector thickness.[13,15,16,20,35]

$$\mathrm{CCE} = \frac{Q_{\mathrm{coll}}}{Q_{\mathrm{gen}}} = \frac{d}{L} \tag{5.6}$$

The charge collection efficiency depends on the applied electric field. At higher electric fields charges have higher velocity and will travel a longer distance before being trapped. The charge collection efficiency increases with increasing field strength and will be at its largest at the field that gives the highest carrier velocity. Semiconductor detectors are usually operated at the highest field possible, with a clear safety margin to any breakdown limit, in order to get the maximal signal and charge collection efficiency.[13]

The next section describes how charge collection distance is measured. The setup and the measurement procedure used in the quality assurance is described in Section 5.3.2. Something to be noted is that for polycrystalline materials the measurement will give the mean charge collection distance. Because of their columnar structure, charge collection distance of polycrystalline materials will vary with the distance from growth surface. The charge collection distance is largest closest to the growth surface and zero at the bottom, where the grain size is the smallest and many boundaries act as traps.[34]

5.3.1 Measurement of charge collection distance and efficiency

Charge collection distance is measured with transient current techniques (TCT). TCT is based on measurement of the current induced by the drift of generated charge carriers, and is a powerful method to study electrical properties of semiconductor materials.[46] Determination of charge collection distance requires knowledge of the number of generated electron-hole pairs inside the detector.[14] Characterization measurements are usually done with minimum ionizing particles (MIP), that deposit the least amount of energy possible (see Section 2.1). The principle of charge collection determination is to measure the amount of charge produced by a single high energy particle.[18] In diamond MIPs produce on average 36 electron-hole pairs per µm.[14,24,47] Assuming the particle arrives perpendicularly to the surface, the charge produced by a MIP travelling through a diamond detector of thickness L is

given by

$$Q_{\text{gen}} \approx 36Le, \tag{5.7}$$

where e is the elementary charge. The charge measured in the circuit Q_{coll} is proportional to the charge collection distance d.

$$Q_{\text{coll}} = Q_{\text{gen}} \frac{d}{L} \tag{5.8}$$

Therefore, the charge collection distance is obtained by measuring the charge produced by one high energy particle.[13–15,18] From the collected charge one can then determine the charge collection efficiency using Equation 5.6. However, in practice is it very difficult to know the generated charge exactly. It is therefore more practical to determine the collected charge relative to a reference sample. Then the CCE is the fraction of the collected charge from the sample to the collected charge from the reference.[1]

$$\text{CCE} = \frac{Q_{\text{coll,sample}}}{Q_{\text{coll,reference}}} \tag{5.9}$$

When measuring the charge collection distance and efficiency one would ideally use minimum ionizing protons or pions that have low energy deposition and undergo little multiple scattering as they traverse the detector. However, their use is not practical, or even possible, in routine measurements.[13,14] Instead, measurements are done using electrons emitted by radioactive sources. Electrons from β-decay have continuous energy distribution with an endpoint energy characteristic for the source. Generally, sources with high endpoint energy give better measurement results. Of course the source has to have a half-life practical for the measurement.[14,15] The activity should be high enough to result in reasonable measurement times, but also not too high to avoid pileup effects.[13] A typical source choice is ^{90}Sr which decays to ^{90}Y. Both isotopes undergo β^--decay.[14,15,18] The endpoint energies of ^{90}Sr and ^{90}Y are 0.55 MeV and 2.28 MeV, respectively. The measurement is done with the 2.28 MeV electrons that have a specific energy loss close to that of MIPs.[34,38,48] ^{90}Sr has some benefits that other isotopes don't have. Neither ^{90}Sr nor ^{90}Y emit gamma rays that cause background to the measurement, and the energy distributions of the electrons are quite narrow. Also, because of the relatively long half-life of ^{90}Sr (28.80 yr), the activity remains almost constant over the years. The half-life of ^{90}Y is 64.5 hr.[13,48]

Electrons with energy less than 0.5 MeV will stop in a 500 µm thick diamond. Therefore the 0.55 MeV electrons will be almost completely stopped in the diamond

and only the 2.28 MeV electrons trigger the measurement. As previously mentioned, these electrons have energy deposition close to that of MIPs. Using the Bethe-Bloch formula (Equation 2.1), with $I_0 = 78\,\text{eV}$ and $v/c \approx 0.957$, one gets that the energy deposition (dE/dx) of MIPs is approximately 1.84 MeV/(g/cm^2) in diamond. The corresponding value in silicon is 1.66 MeV/(g/cm^2). The number of electron-hole pairs (N_{eh}) produced in a detector of thickness L is given by

$$\frac{N_{\text{eh}}}{L} = \frac{\frac{dE}{dx}\rho}{E_{\text{eh}}}, \tag{5.10}$$

where ρ is the material density and E_{eh} the energy required to produce one electron-hole pair. Using the values in Table 3.1 the number of generated electron-hole pairs N_{eh}/L is 49.5 pairs/µm in diamond and 107.4 pairs/µm in silicon. The Bethe-Bloch assumes that all the energy deposited by the incident particle goes to generation of electron-hole pairs. However, in thin detectors energetic secondary particles can escape from the detector carrying off part of the energy. The energy loss of MIPs is smaller than given above. To get the energy deposition one has to use a modified Bethe-Bloch formula (see Equation 2.5 in Reference [47]). The energy deposition is 1.34 MeV/(g/cm^2) in diamond and 1.23 MeV/(g/cm^2) in silicon. Now the number of generated electron-hole pairs N_{eh}/L is 36.1 pairs/µm in diamond and 69.6 pairs/µm in silicon. These values can then be used to calculate the number of electron-hole pairs produced in a detector with a certain thickness. A MIP passing through a 500 µm diamond will produce 18 000 electron-hole pairs. The corresponding value in silicon is 40 000, a factor of 2.2 larger than in diamond.[47]

5.3.2 Measurement setup and process

The setup for measurement of charge collection efficiency and distance consists of four main parts: the detector under test (DUT), a trigger detector, typically a silicon detector, a radiation source, usually ^{90}Sr, and electronics for signal readout. The trigger detector is typically a silicon detector and it is used to start the data acquisition when certain requirements are fulfilled. The electrons from the source are emitted randomly and there are signals from the background. To guarantee that the detected electron is from the radiation source, the particle has to be detected in both the DUT and the trigger detector.[13,15,34,38] Due to scattering and absorption in the diamond detector, most low energy electrons emitted by the source will not reach the active volume of the trigger detector. An energy threshold is used to make sure that the low energy electrons that reach the active volume of the trigger detector,

don't start the data acquisition.[14,15,38] The radiation source is collimated in order to minimize effects of multiple scattering, and to make sure that electrons triggering the measurement travel through the DUT in a nearly straight line.[13] The energy threshold and the collimator guarantee that the electrons triggering the measurement can be approximated as MIPs.[14,38]

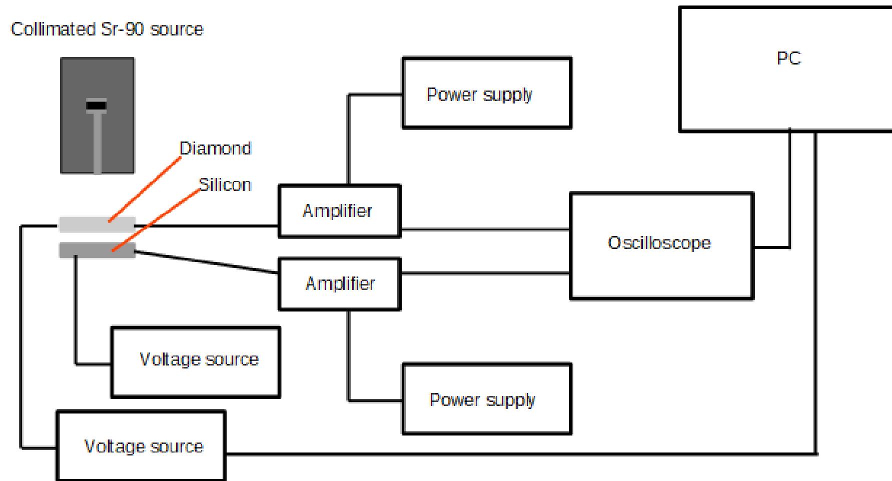

Figure 5.8: The setup for the charge collection efficiency measurement.

The setup used in the quality assurance measurements is sketched in Figure 5.8. The diamond is placed on top of a N-type silicon pad detector underneath a ^{90}Sr-source. The source used in this work is well focused and there are only small variations in the angle the electrons leave the source. Therefore, the angle at which the electrons leave the source has only a small effect on the angle at which they enter the diamond, unless the source is very close to the sample. All electrons, except those measured right under the source, are scattered electrons. The source opening is about 1 cm, which is large compared to the sample size. The silicon detector is very sensitive to light, which is why it is placed inside a shield made of black plastic. Both detectors are connected to Cividec instrumentation Diamond Charge Amplifier CSA1 fast charge sensitive amplifiers, that are connected to the Teledyne Lecroy wavepro 7300A 3Ghz oscilloscope. The power to the silicon detector and the amplifiers are supplied by Iso-Tech IPS303DD Laboratory and Velleman PS613 DC power supplies. The power to the diamond is supplied by a Keithley 2410 source meter. The diamond is biased from the bottom and read out from the top, while the trigger detector is biased from the top and read out from the bottom. The Keithley and the oscilloscope are connected to the measurement computer. The data is collected with custom made software based on MATLAB. The software also controls the diamond bias voltage. Both detectors, the amplifiers and the ^{90}Sr-source

are placed inside a dark box and all measurements are done in a dark room in order to reduce the background due to surrounding light. The box is also a radiation safety box. Lead plates in the walls of the box keep the radiation inside and protect the environment from radiation. Enclosing the setup in a box guarantees that long measurements can be performed in a safe manner without changes in the setup.

The measurement is performed by increasing the voltage from 100 V to 1000 V in 50 − 200 V steps. Diamond is quite sensitive to polarization. For results not to be affected by the polarization, the measurements need to be short and the bias voltage turned off periodically[2,7]. The diamond signals are read from the oscilloscope whenever the silicon signal exceeds a certain trigger level. The signal amplitude and shape vary because the electrons traversing the detector have different energy. Variations in the signal are also caused by Landau fluctuations. The diamond detector is thin, so the electrons pass through the detector and deposit only a fraction of their total energy. Random variations in the number of collisions and the energy transfer in each collision lead to variations in the energy deposition of each electron. Additional variations in the deposited energy are due to variations in the angle of incidence. The electrons enter the diamond in different angles and therefore pass through different thickness of material and deposit different amount of energy in the detector. 500 signals are collected at every voltage step in order to form a mean signal shape and to get the variation for every position in the signal. The mean signal is then used to determine the maximum signal amplitude, the collected charge, CCE and charge carrier velocity. The measurement results are compared with results obtained with the reference sample using the same measurement conditions and settings. Therefore the reference sample has to be measured every time the setup is changed or the trigger modified. These measurements have not been performed routinely as part of the quality assurance process before. Hence, the rejection criteria will be determined after the first 15 samples.

In order to get a complete picture of the sample and to find any variations in charge collection, CCE is measured at different positions on the the diamond. After the first metallization, the CCE is measured at five different positions, in all four corners and in the middle. After metallization of the strips, the CCE is measured at four positions on every strip, leading to a total of 16 measurement positions. Both measurement geometries are shown in Figure 5.9. In the previous setup the measurement was manually changed after every measurement. Every time the measurement position was changed the radiation source had to be removed and the new position found using a removable light source (not visible in Figure 5.8). The

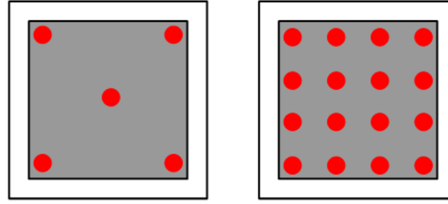

Figure 5.9: Measurement positions in the CCE measurement after the first metallization (left) and after metallization of the strips (right).

new measurement position was found by placing the light source where the ^{90}Sr-source is during the measurement and moving the source holder until the light was in the correct location on the diamond. Once the source holder was in the correct position, the light source was removed and the ^{90}Sr-source put back on the source holder. This isn't a very accurate and fast way to select the measurement position and leads unavoidably to inconsistencies in the separation between measurement positions. In addition, the manual method is time consuming. Therefore, a stage controller was built to improve the accuracy of the scanning and to make the measurement more automatic. In addition to the improved accuracy of the positioning, the stage controller reduces the radiation dose the person doing the measurement is exposed to since the measurement requires less handling of the radiation source. Both detectors and the amplifiers are placed on top of the stage controller and the ^{90}Sr-source is placed at the first measurement position using a light source. When the measurement is started the stage controller will automatically move to all defined positions and perform the measurement as described above. The stage controller is moved by an Arduino interfaced to the data acquisition software, and can be used to measure several samples in one run. An Arduino is an electronics board that can read inputs and turn them into outputs. The instructions are sent by a microcontroller (a small "computer" embedded in the device controlling its features or actions) using Arduino software[49]. In this case the Arduino controls the power to two stepper motors. The parts of the stage controller and its operation are described in Appendix A.

The setup was tested by measuring the signals from a reference diamond at the five positions show on the left in Figure 5.9. The voltage was changed from 100 V to 1000 V in 200 V steps. The trigger was placed well above the noise level in order to get good signals from both the silicon and diamond. The signal was noisy so the trigger had to be placed quite high, at approximately 26 mV, on the positive edge of the silicon detector signal. The stability of the setup and the reproducibility of the result were tested by performing 20 measurements with the same measurement settings and measurement conditions. The trigger and the voltage scan interval were

the same as in the test run. But in the reproducibility measurements the voltage step was set as 100 V. The reproducibility measurements were done during a time period of eight days. All measurements were done in ambient conditions. The measurement conditions were neither monitored nor controlled during the measurements.

6. Results

This chapter presents the results of the test run and the reproducibility measurements. Unfortunately, due to delays in the processing, no metallized samples were available in time for this thesis. Therefore the setup and quality assurance procedure could not be tested with actual samples. Instead the procedure for the quality assurance measurements is demonstrated with two consecutive measurements on the reference sample from the reproducibility measurements.

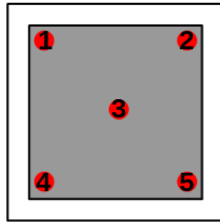

Figure 6.1: Positions 1–5 to be measured on the diamond detector.

The measurements were taken for five positions of the sample. Positions 1, 2, 4, and 5 are in the corners of the diamond and position 3 in the center, see Figure 6.1. Figure 6.2 shows the averaged waveforms measured at different voltages in all five positions. The signal is formed by charge carriers generated by the ionizing electrons from the radiation source passing through the diamond. The setup measures both charge carriers, for which the signal shapes are almost identical. The maximum signal amplitudes are plotted as function of the diamond bias voltage in Figure 6.3. The uncertainty was estimated as the standard deviation of the collected waveforms at the location of the signal maximum ($\mathrm{Std}(A_{\mathrm{max}})$) divided by the square root of the number of waveforms (N)[50].

$$\sigma_{\mathrm{A_{max}}} = \frac{\mathrm{Std}(A_{\mathrm{max}})}{\sqrt{N}} \tag{6.1}$$

In all positions except position 5 the amplitude increases with higher voltage until a plateau is reached in the middle of the voltage range. In positions 1 and 4 the amplitude decreases at a certain voltage. For position 4 the amplitude increases again at the end of the voltage range. In position 5 the amplitude decreases after the

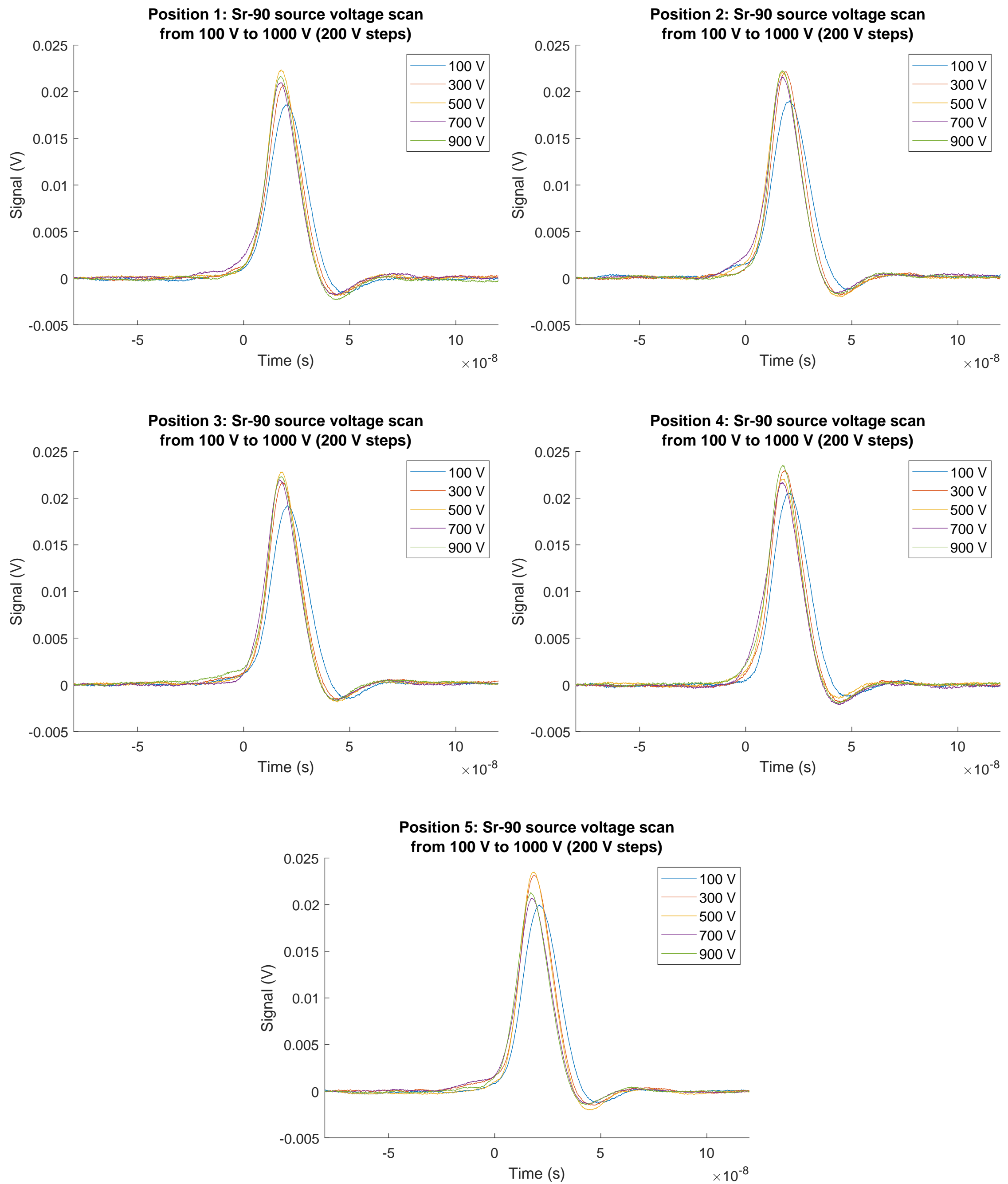

Figure 6.2: Averaged waveforms of 500 measurements with ^{90}Sr-source measured at five different positions according to Figure 6.1 on the reference diamond for different voltages.

initial increase and remains on the same level until the end of the voltage range.

From the signal duration one can determine the charge carrier drift velocity v. The drift velocity is given by

$$v = \frac{L}{t_\mathrm{d}}, \tag{6.2}$$

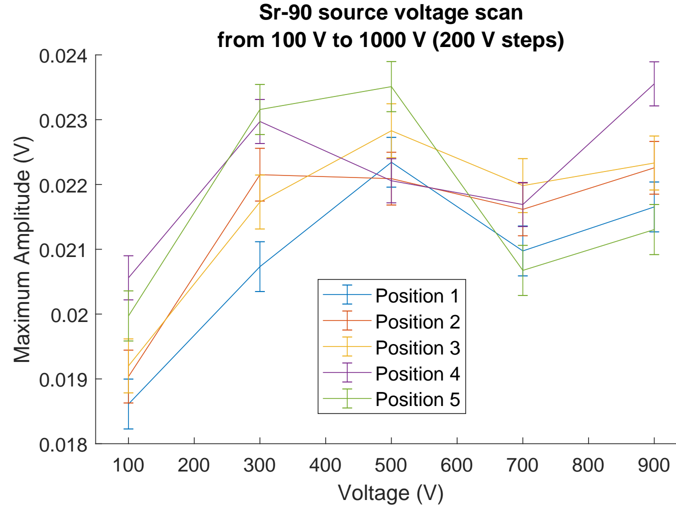

Figure 6.3: Maximum signal amplitude as function of bias voltage. The bars denote the uncertainty of the signal maximum estimated with Equation 6.1.

where L is the detector thickness (500 µm) and t_d the drift time. In order to have comparable measurements, the drift time was defined in the same way as in Reference [2]. The drift time is defined as the time from 20 % of the signal maximum (A_max) on the rising edge (t_1) to the 15 % of the signal maximum on the falling edge (t_2).

$$t_\mathrm{d} = t_2 - t_1 \tag{6.3}$$

The uncertainty of t_1 was estimated as the average of the time from $0.20 \cdot (A_\mathrm{max} - \sigma_{\mathrm{A_{max}}})$ to $0.20 \cdot A_\mathrm{max}$ and the time from $0.20 \cdot A_\mathrm{max}$ to $0.20 \cdot (A_\mathrm{max} + \sigma_{\mathrm{A_{max}}})$ on the rising edge. The uncertainty of t_2 was estimated similarly as the average of the time from $0.15 \cdot (A_\mathrm{max} + \sigma_{\mathrm{A_{max}}})$ to $0.15 \cdot A_\mathrm{max}$ and the time from $0.15 \cdot A_\mathrm{max}$ to $0.15 \cdot (A_\mathrm{max} - \sigma_{\mathrm{A_{max}}})$ on the falling edge. The uncertainty of the drift time and velocity were obtained with the equation of error propagation[50].

$$\sigma_f = \sqrt{\left(\frac{\partial f}{\partial x}\right)^2 \sigma_x^2 + \left(\frac{\partial f}{\partial y}\right)^2 \sigma_y^2 + \dots} \tag{6.4}$$

Figure 6.4 shows the calculated drift velocity as function of the applied electric field. The velocities in position 1, 2 and 3 increase with higher electric field until a plateau is reached in the middle of the electric field range. In all positions the velocity decreases slightly at 1.4 V/µm. In position 2 the velocity increases again at the end of the electric field range. The velocity changes are similar in positions 4 and 5. The velocity increases with higher electric field until a certain point in the

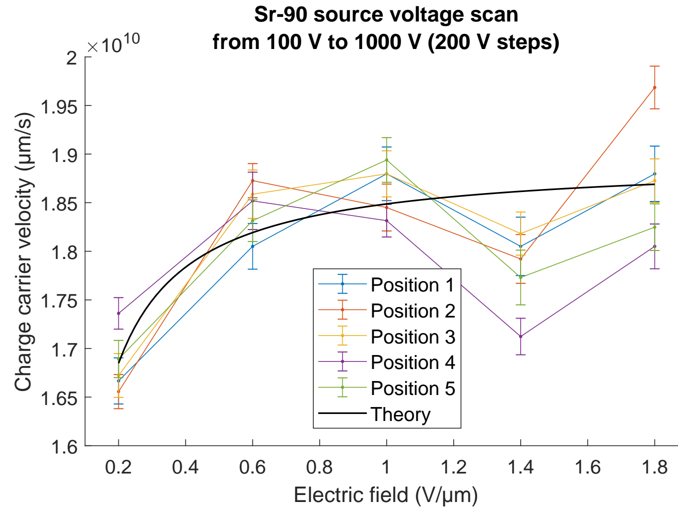

Figure 6.4: Charge carrier velocity as function of applied electric field. The bars denote the uncertainty calculated with Equation 6.4. The black curve is the theoretical value for the velocity calculated with Equation 2.5 using the mean values in Table 6.1.

middle of the electric field range, after which the velocity starts to decrease. The decrease is quite large at 1.4 V/µm. The velocity increases again at the end of the electric field range, but not as high as before the decrease.

The detector saturation drift velocity and low field mobility were determined by fitting Equation 2.5 to the measured velocity. The fit is made in such a way that the fit parameters correspond to μ_0 and v_{sat} in the equation. The parameters were determined for all positions, from which means were calculated. The uncertainties were calculated from the 1σ confidence limits determined by the curve fit function in MATLAB. The obtained results are presented in Table 6.1. The values for the saturation velocity are similar for all positions except position 4, in which the saturation velocity is lower. The low field mobility is also much larger in position 4 than in the other positions. Due to the large difference, parameter values for position

Table 6.1: Low field mobilities and saturation drift velocities obtained by fitting Equation 2.5 to the measured velocities.

	μ_0 [cm^2/(Vs)]	σ_{μ_0} [cm^2/(Vs)]	v_{sat} [cm/s]	$\sigma_{v_{sat}}$ [cm/s]
Position 1	7100	±2100	$1.890 \cdot 10^6$	$\pm 0.032 \cdot 10^6$
Position 2	6000	±3000	$1.926 \cdot 10^6$	$\pm 0.063 \cdot 10^6$
Position 3	7400	±2300	$1.901 \cdot 10^6$	$\pm 0.032 \cdot 10^6$
Position 4	30000	±9600	$1.807 \cdot 10^6$	$\pm 0.052 \cdot 10^6$
Position 5	9900	±6000	$1.861 \cdot 10^6$	$\pm 0.047 \cdot 10^6$
Mean[1]	7600	±1900	$1.895 \cdot 10^6$	$\pm 0.023 \cdot 10^6$

[1] The low field mobility and saturation velocity in position 4 are excluded from the mean values.

4 were excluded in the calculation of the mean values. The difference is explained by the slightly different behaviour of the velocity in position 4. According to the theoretical model (Equation 2.5), the velocity should increase at low fields until the velocity saturates and becomes constant. In all positions the velocity drops at some point, but all positions except position 4 show a clear increase in the beginning of the electric field range. Also, in position 4 the decrease in the middle of the range quite large and the velocity doesn't increase back to the values observed at low electric fields. The black curve in Figure 6.4 is the velocity calculated with Equation 2.5 using the mean values for the low field mobility and the saturation velocity presented in Table 6.1. The measured velocity matches quite well with the theoretical value until the drop at 1.4 V/µm. Typical values for the low field mobility and saturation drift velocity are shown in Table 3.1. The obtained low field mobility is higher than the mobility typically measured in diamond. The saturation drift velocity on the other hand is lower than the typical value in diamond.

The effective mobility, i.e. the observed mobility, μ was obtained by solving Equation 2.4. By writing the velocity v with Equation 6.2 and the electric field strength $E = V/L$ the effective mobility becomes

$$\mu = \frac{L^2}{V t_\mathrm{d}}. \tag{6.5}$$

Figure 6.5 shows the effective mobility at different electric fields. The uncertainty was calculated with the error propagation formula (Equation 6.4). As expected,

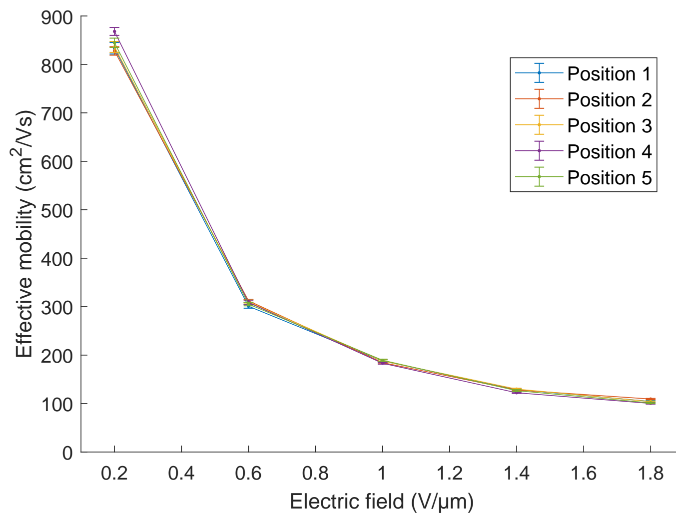

Figure 6.5: The observed mobility calculated with Equation 6.5 at different electric fields. The bars show the uncertainty calculated with Equation 6.4.

the effective mobility decreases with higher electric fields. The effective mobility decreases from about 800 $cm^2/(Vs)$ to about 100 $cm^2/(Vs)$. As described in Section 2.2, the charge carrier velocity saturates at high electric field strengths due to increased scattering of charge carriers and space charge effects. The mobility is proportional to the charge carrier velocity. Therefore, the mobility will decrease as the velocity increases at higher electric field strengths. The linear equation used in these calculations doesn't consider effects that reduce the mobility. Therefore the calculated effective mobility is only an approximation of the true effective mobility. To include these effects Equation 6.5 has to be modified such that it contains the voltage (V_c) required to compensate for the space charge effects. V_c is determined from the "knee" in a collected charge (Q) vs square root of voltage ($\sqrt{V}$) plot. In these measurements the voltage was not low enough to observe a knee, hence the effective mobility was approximated with the linear equation. In Reference [7] the effective mobility of a single crystal CVD diamond is determined using the equation accounting for space charge effects and charge carrier scattering.

Integration of the waveforms over time gives the collected charge. Here the collected charge was estimated as the sum of the product of the signal at a certain time t ($A(i)$) and time step ($\mathrm{d}t = t(i+1) - t(i)$) over the whole signal duration.

$$Q \approx \sum_i (A(i) \cdot \mathrm{d}t) \tag{6.6}$$

A mean was calculated of the charge calculated for each waveform. Figure 6.6 shows the mean collected charge at different voltages. The uncertainty was estimated as

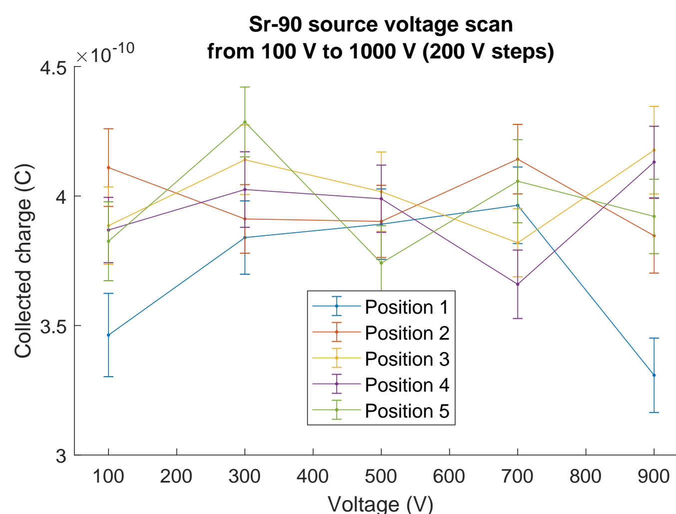

Figure 6.6: The collected charge at different voltages. The bars show the uncertainty calculated with Equation 6.4.

the standard deviation of the collected charge (Std(Q)) divided by the square root of the number of waveforms (N) used in the analysis.

$$\sigma_{\mathrm{Q}} = \frac{\mathrm{Std}(Q)}{\sqrt{N}} \tag{6.7}$$

The collected charge was expected to increase with higher voltage, but this was not observed in the measurement. In all positions, except position 1, the collected charge fluctuates around a constant value. In positions 3 and 4 the collected charge decreases slightly at 700 V. In position 5 the collected charge fluctuates more in the beginning of the voltage range. In position 1 the collected charge increases until it reaches a plateau in the middle of the voltage range. The collected charge decreases at the end of the voltage range.

The charge collection efficiency was determined from the collected charge using Equation 5.6 and its uncertainty with Equation 6.4. However, since this was the first measurement done with the setup with these settings, no reference value for the collected charge was available. Instead the position with the highest collected charge per voltage step was set as reference and the other values compared to it. The results are shown in Figure 6.7 and Table 6.2. The charge collection efficiency is over 80 % in all positions and voltages except in position 1 at 900 V, which means that the collected charge is similar in all positions over the whole voltage range.

Table 6.2: Charge collection efficiency in the measurement positions at different voltages.

	100 V [%]	300 V [%]	500 V [%]	700 V [%]	900 V [%]
Position 1	84.27±4.98	89.59±4.34	96.87±5.01	95.70±4.73	79.19±4.70
Position 2	100.00±5.17	91.27±4.22	97.14±5.07	100.00±4.58	92.09±5.08
Position 3	94.55±5.01	96.60±4.36	100.00±5.39	92.21±4.36	100.00±5.73
Position 4	94.13±4.61	93.92±4.51	99.32±4.98	88.34±4.29	98.90±5.20
Position 5	93.08±5.03	100.00±4.45	93.13±5.05	97.95±5.01	93.88±5.13

The reproducibility measurements were used to determine how the signal amplitude, collected charge and charge carrier velocity change over time and how similar the results in different positions are compared to each other. Figures 6.8, 6.9 and 6.10 show examples of the measured trends. The mean for all 20 measurements is marked with a black line. The dashed line in red is the uncertainty of the mean obtained by considering the uncertainty of the result in each measurement (σ_1, σ_2,. . . , σ_{N}) and the number of observations ($N = 20$)[50].

$$\sigma_{\mathrm{mean}} = \sqrt{\left(\frac{\sigma_1}{N}\right)^2 + \left(\frac{\sigma_2}{N}\right)^2 + \cdots + \left(\frac{\sigma_{\mathrm{N}}}{N}\right)^2} \tag{6.8}$$

The dashed line in black is the standard deviation of the parameter and it describes how close to the mean the measurement results are. The variation of the results was determined by dividing the standard deviation of the 20 measurements with their mean. The results of the reproducibility measurements are tabled in Appendix B. All five positions have similar means for the maximum amplitude, charge carrier velocity and collected charge at different voltages. Most measurements have similar standard deviation for the maximum amplitude and charge carrier velocity. In some measurements the mean and standard deviation are slightly different due to a couple of individual measurements with slightly smaller or larger results. The variation between measurements seems large, but this is only due to the scale on the y-axis. The variation between the results is less than 6.0 % for the maximum signal amplitude and less than 3.5 % for the charge carrier drift velocity. For the collected charge the variation between measurements is less than 8.5 %. The mean collected charge and the standard deviation of the results are similar in all measurements. Overall, the results for the maximum amplitude, collected charge and carrier velocity are stable in all positions over the whole measured voltage range.

Figure 6.11 shows an example trend for the charge collection efficiency. The trends were formed by setting the position with the highest average collected charge at each voltage as the reference value and comparing the charge collected in each

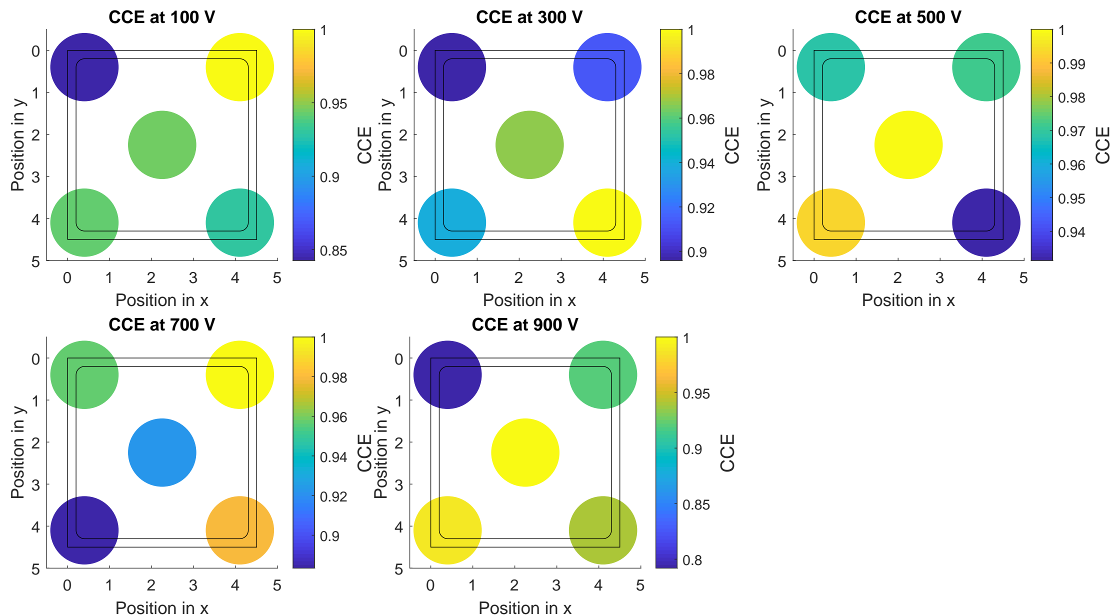

Figure 6.7: Charge collection efficiency at five positions at different voltages. The charge collection efficiency was determined by comparing the collected charge in every position to the position with the highest collected charge using Equation 5.6

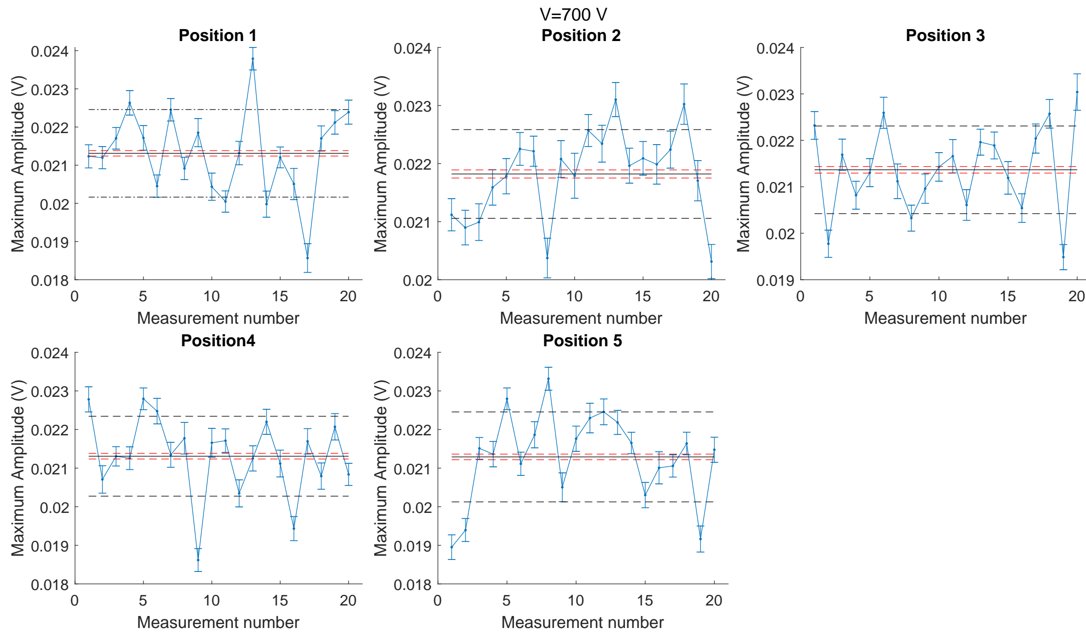

Figure 6.8: Trend lines for the maximum amplitude determined in the reproducibility measurements at 700 V. The mean is marked with a black line. Its calculated uncertainty (red) and the standard deviation of the measured values (black) are marked with dashed lines.

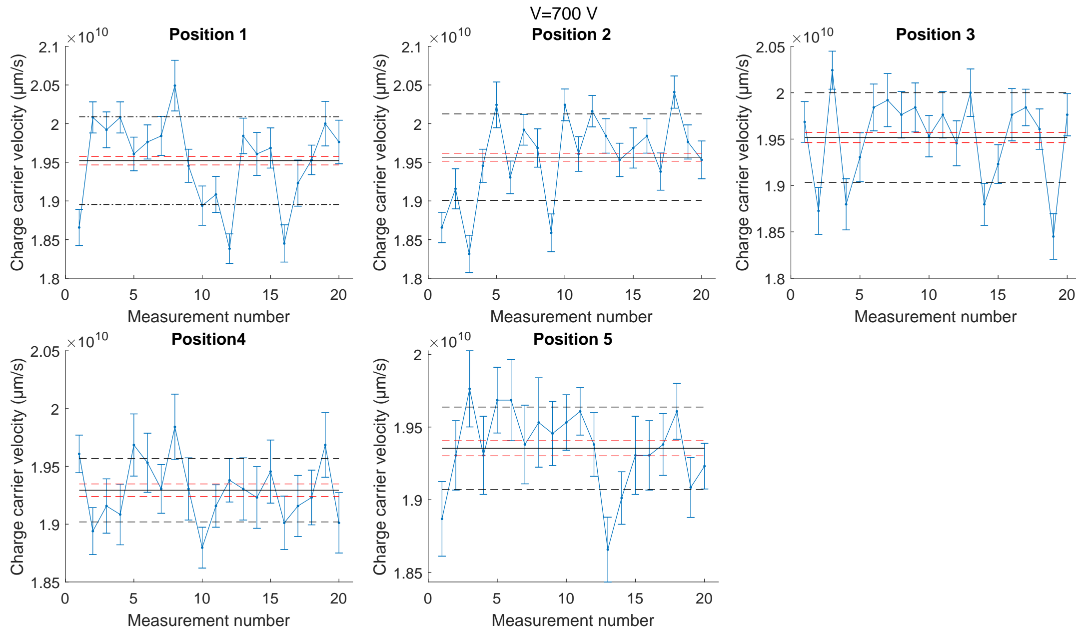

Figure 6.9: Trend lines for the charge carrier velocity determined in the reproducibility measurements at 700 V. The mean is marked with a black line. Its calculated uncertainty (red) and the standard deviation of the measured values (black) are marked with dashed lines.

measurement to it using Equation 5.6. The uncertainty was calculated with Equation 6.4 considering the uncertainty of the measured collected charge and the uncertainty

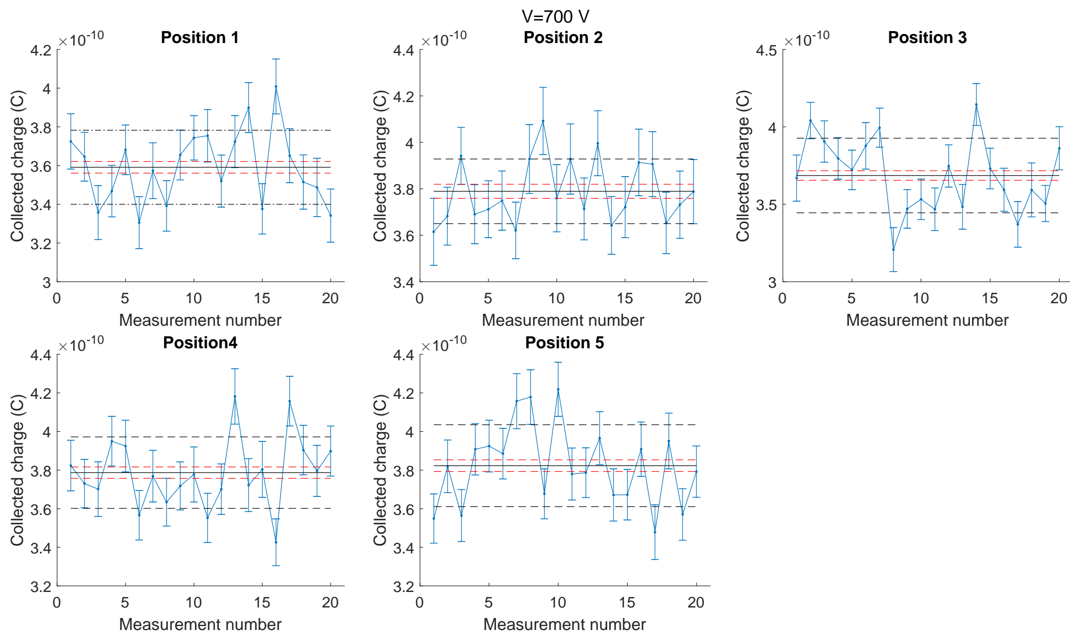

Figure 6.10: Trend lines for the collected charge determined in the reproducibility measurements at 700 V. The mean is marked with a black line. Its calculated uncertainty (red) and the standard deviation of the measured values (black) are marked with dashed lines.

of the highest mean value. By comparing all positions to the same value, the mean in this case, one can find out whether the CCE depends on the position. The mean of the 20 measurements is marked with a black line. The dashed line in red is the uncertainty of the mean calculated with Equation 6.8 by considering the uncertainty of each measurement. The dashed line in black is the standard deviation of the results. The standard deviations, the means and their uncertainty are tabled in Appendix B. As can already be seen from the trends for the collected charge, the charge collection efficiency changes between measurements. The fluctuations seem large due to the scale on the y-axis, but the difference between the collected charges is not that large. At most voltages the means and standard deviations are similar in all positions. Only a few positions have slightly different mean and standard deviation compared to the other positions at a certain voltage. The variation of the CCE was studied by counting how many measurements fall in certain CCE ranges in every position. In all positions all measurements, except one at 900 V, have CCE between 85 % and 115 %, and most measurements between 90 % and 110 % at all voltages. At all voltages in most positions at least half of the measurements have CCE between 95 % and 105 %. This means that the charge collection efficiency doesn't change much over time. Also, the CCE doesn't depend on the position because the means and the distribution of the results is similar in all positions.

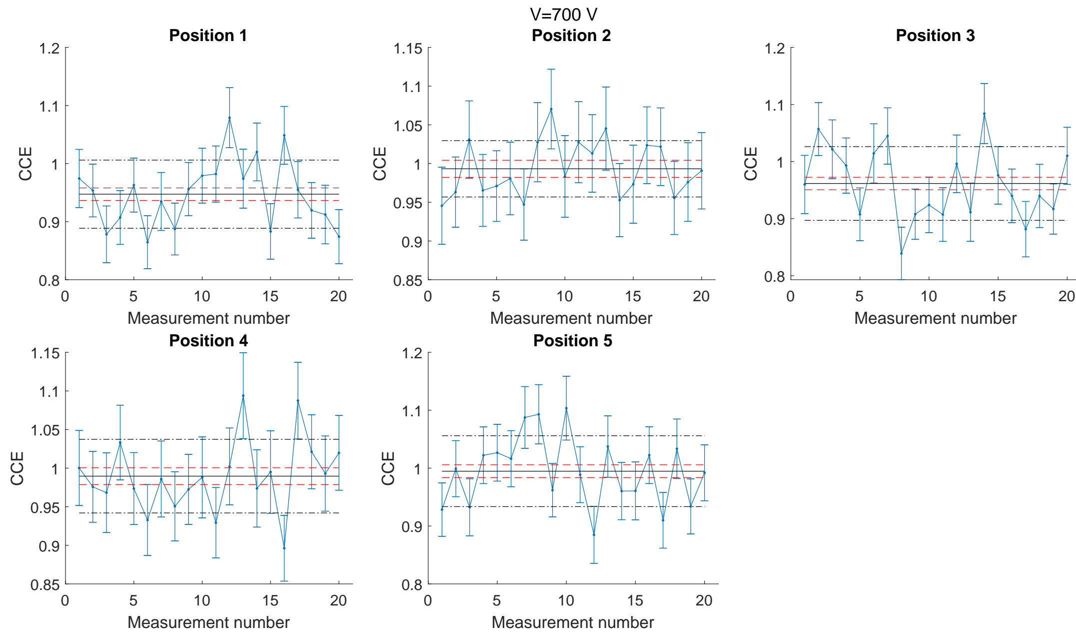

Figure 6.11: Charge collection efficiency for the reproducibility measurements at 700 V. The trends were formed by comparing the charge collected in every measurement to the highest mean collected charge at each voltage. The bars show the uncertainty of the charge collection efficiency calculated with Equation 6.4. The mean of the 20 measurements is marked with a black line. Its calculated uncertainty (red) and the standard deviation of the measured values (black) are marked with dashed lines.

6.1 Quality assurance measurements

As mentioned earlier, no metallized samples were available in time for this thesis, so the quality assurance procedure is demonstrated with the second measurement in the reproducibility measurements. The first measurement was set as reference. All calculations were done as described previously in this chapter.

Figure 6.12 shows the measured maximum signal amplitude at different voltages. In position 1 the amplitude increases up to 400 V, after which the amplitude varies around a smaller value. In position 4 the amplitude increases up to 500 V. After a quite large decrease, the amplitude increases steadily back to the level it was before the decrease. In positions 1 and 4 the amplitude at 1000 V is higher than at 100 V. In position 2, 3 and 5 the amplitude fluctuates around a constant value over the whole voltage range. The fluctuations are large at lower voltages in position 2. The maximum amplitude is the most stable in position 5.

The charge carrier velocity as a function of the applied electric field is shown in Figure 6.13. The black curve is the theoretical velocity calculated with Equation 2.5 using the mean low field mobility and saturation drift velocity presented in Table

6.3. The velocity doesn't decrease in all positions at a certain electric field like in the test run, but the velocity varies more at higher electric fields. In position 1, 3 and 5 the velocity increases with higher electric field until it starts to fluctuate around a constant value. The velocity in positions 3 and 5 fluctuate more in the middle and at the end of the electric field range, respectively. In position 2 the velocity increases up to 1.0 V/µm, after which the velocity decreases with higher electric field. In position 4 the the velocity increases with higher electric field, except for a slight decrease in the middle of the electric field range. The measured velocity follows the theory better than in the test run. Table 6.3 lists the low field mobility and saturation velocity values obtained from the fits of Equation 2.5. The saturation velocity is similar in all positions. The mean saturation velocity is slightly larger than the velocity obtained in the test run. The low field mobility varies between measurement points but not as much as in the test run. The mean low field mobility is smaller than in the test run. Even though the saturation velocity is higher and

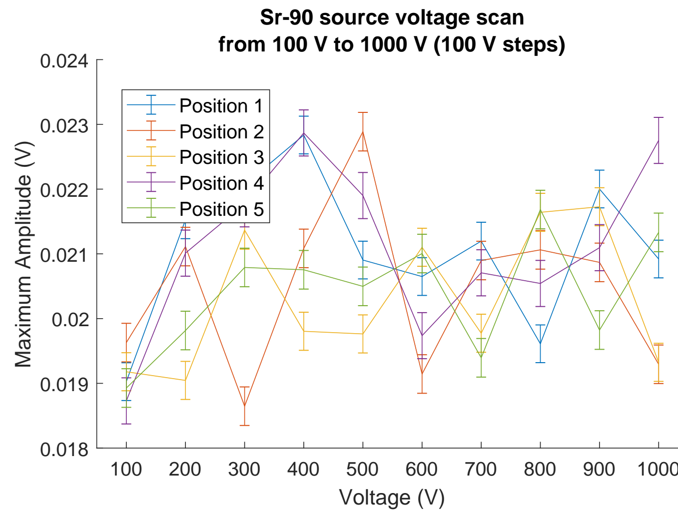

Figure 6.12: The maximum signal amplitude and its calculated uncertainty as function of bias voltage in the second reproducibility measurement.

Table 6.3: Low field mobility and saturation drift velocity obtained by fitting Equation 2.5to the measured velocities in the second reproducibility measurement.

	μ_0 [cm^2/(Vs)]	σ_{μ_0} [cm^2/(Vs)]	v_{sat} [cm/s]	$\sigma_{v_{sat}}$[cm/s]
Position 1	7100	±1516	$1.988 \cdot 10^6$	$\pm 0.021 \cdot 10^6$
Position 2	9100	±3393	$1.964 \cdot 10^6$	$\pm 0.028 \cdot 10^6$
Position 3	6300	±1747	$1.995 \cdot 10^6$	$\pm 0.030 \cdot 10^6$
Position 4	6600	±1772	$1.980 \cdot 10^6$	$\pm 0.027 \cdot 10^6$
Position 5	7800	±3077	$1.969 \cdot 10^6$	$\pm 0.035 \cdot 10^6$
Mean	7400	±1100	$1.979 \cdot 10^6$	$\pm 0.013 \cdot 10^6$

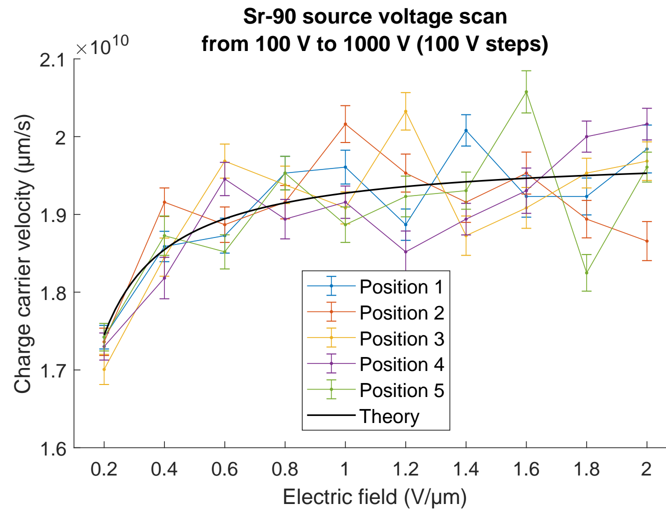

Figure 6.13: Charge carrier velocity and its calculated uncertainty at different electric fields in the second reproducibility measurement. The black curve is the theoretical for the velocity calculated with Equation 2.5 using the mean low field mobility and saturation drift velocity in Table 6.3.

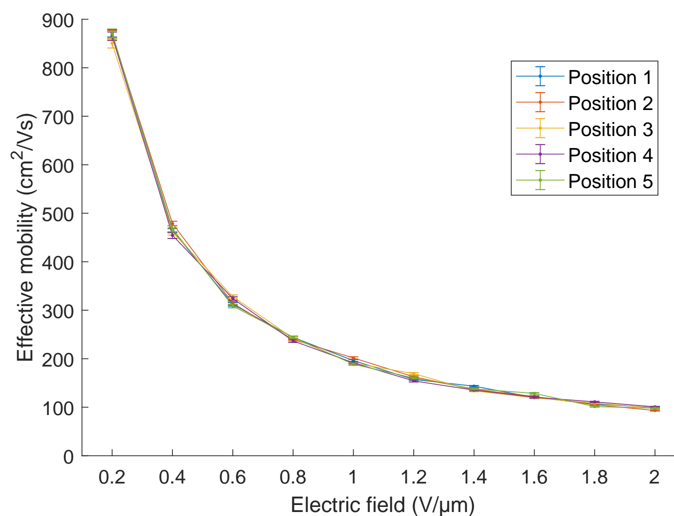

Figure 6.14: The observed mobility and its calculated uncertainty at different electric fields.

the low field mobility smaller than in the test run, the values still don't match with the theoretical values presented in Table 3.1. Scanning with smaller voltage steps reduces the uncertainty of the determined low field mobility and saturation velocity. Just like in the test run, the effective mobility decreases with higher electric fields, see Figure 6.14. Again the effective mobility decreases from about $800\,\mathrm{cm}^2/(\mathrm{Vs})$ to about $100\,\mathrm{cm}^2/(\mathrm{Vs})$ with increasing electric field strength.

The collected charge shown in Figure 6.15 fluctuates between the positions. The difference is largest at low voltages and smallest in the middle of the voltage range. The variation between voltages is quite large and no clear trend can be seen.

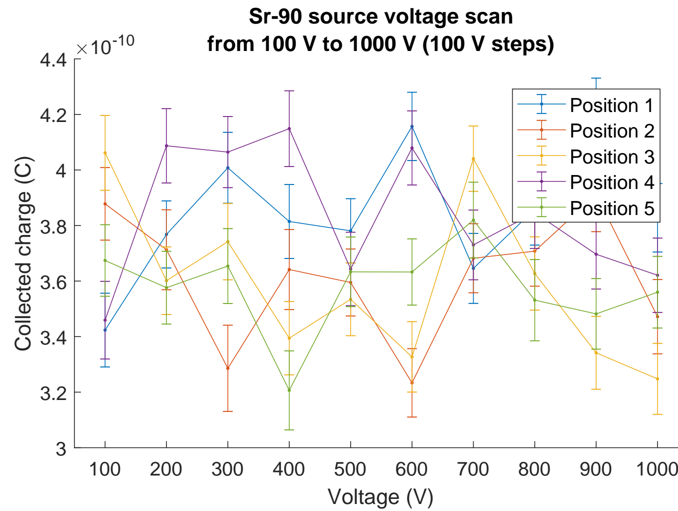

Figure 6.15: Collected charge and its calculated uncertainty at different bias voltages in the second reproducibility measurement.

The collected charge is most stable in position 5. In position 4 the collected charge decreases with higher voltage after an initial increase. In positions 1, 2 and 3 the collected charge varies between higher and lower values.

The collected charge measured in each position was compared to the charge measured in the corresponding position in the reference measurement, in this case

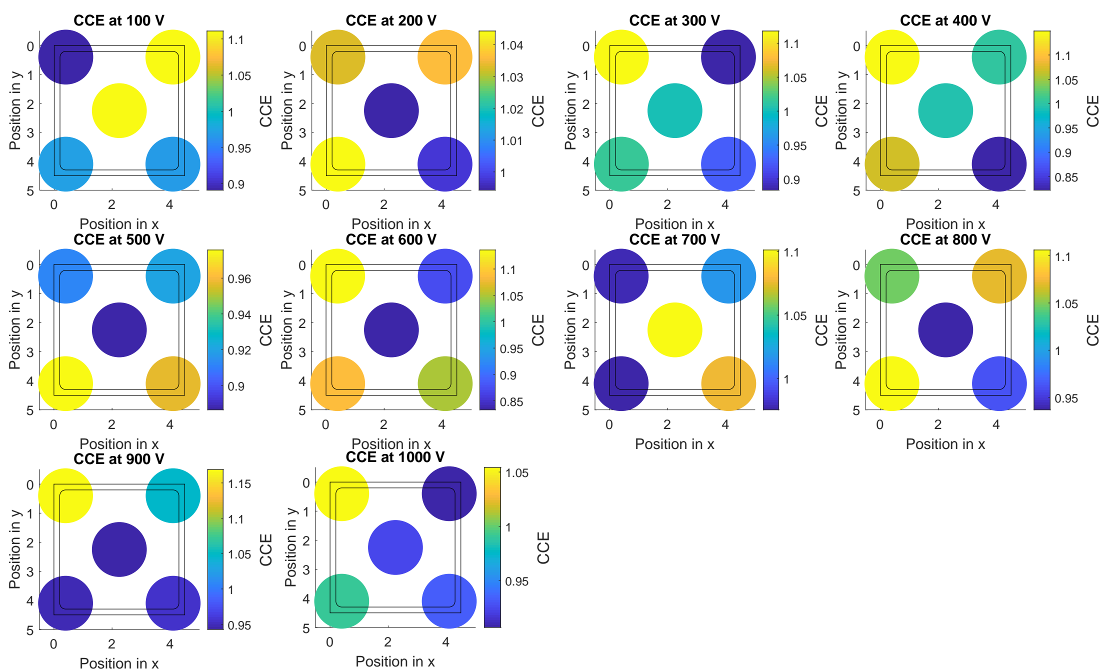

Figure 6.16: Charge collection efficiency in the second reproducibility measurement determined by comparing the collected charge with the charge measured in the first reproducibility measurement.

Table 6.4: Charge collection efficiency in the measurement positions at different voltages.

	100 V [%]	200 V [%]	300 V [%]	400 V [%]	500 V [%]
Position 1	89.10±4.54	103.30±5.10	111.79±5.43	114.92±6.35	91.27±4.11
Position 2	111.08±5.86	103.57±5.79	88.35±5.43	100.43±5.55	92.11±4.47
Position 3	110.90±5.44	99.42±5.19	100.16±5.26	99.40±5.40	88.63±4.60
Position 4	97.19±5.46	104.42±4.87	101.59±4.71	107.16±4.86	97.58±4.67
Position 5	96.97±4.89	99.77±5.08	92.54±4.68	82.18±4.62	95.64±4.72

	600 V [%]	700 V [%]	800 V [%]	900 V [%]	1000 V [%]
Position 1	113.61±5.34	97.87±5.05	104.54±5.36	116.89±5.70	105.41±5.02
Position 2	87.30±4.72	101.87±5.33	106.97±5.31	104.74±5.18	90.71±4.56
Position 3	83.29±4.34	110.12±5.50	93.69±4.53	94.27±5.06	92.54±5.22
Position 4	108.55±5.15	97.55±4.69	110.61±5.52	94.74±4.66	99.09±4.96
Position 5	105.05±5.46	107.62±5.45	96.11±5.26	95.53±4.67	93.34±4.59

the first reproducibility measurement. Table 6.4 lists the charge collection efficiency in all positions at different voltages, relative to the reference measurement. The results are visualized in Figure 6.16. As previously mentioned, the measured collected charge is compared to the collected charge determined in the reference measurement. This means that CCE is smaller than 1 if the measured charge is smaller than the reference value, and larger than 1 if the measured charge is larger than in the reference measurement. In most measurements the charge collection efficiency is about the same or higher than in the reference measurement. Only six measurements have charge collection efficiency less than 90 %. As mentioned in the previous chapter, the rejection limits for the CCE measurements have not been determined yet. The reference measured in this thesis is a diamond that has good electrical properties and will be used as reference in the quality assurance measurements. The reference diamond has good crystal quality. Therefore, one could already say that the coming samples to be tested should have similar or even better charge collection than this reference.

6.2 Reducing the measurement uncertainty

The uncertainty of the signal amplitude was large in the first analyses of the measurement data. The other results are calculated from the averaged signal or from the individual waveforms, so uncertainties and variations of the amplitude are propagated to the other results. In the results presented in this thesis the uncertainties have

been significantly reduced, but they could be reduced even further. The results also vary between measurements. The standard deviation of the results is larger than the uncertainty of the measurement, which means that statistical variations in each measurement are not the only source of uncertainty. This section describes the efforts done to reduce the measurement uncertainty. Sources of the variation were not studied.

The first step was to find the source of the uncertainty. Since the large uncertainty is seen already in the averaged signal, the search was started from the 500 waveforms forming the averaged signal. Figure 6.17a shows an example of one set of 500 waveforms measured in position 1 at 1000 V. A closer look at the signals revealed that there are many bad signals among the good signals. Some signals have rectangular or step like form. Often there is no signal from the diamond when the silicon detector triggers the measurement. Also, the maximum amplitude of the signal varies a lot.

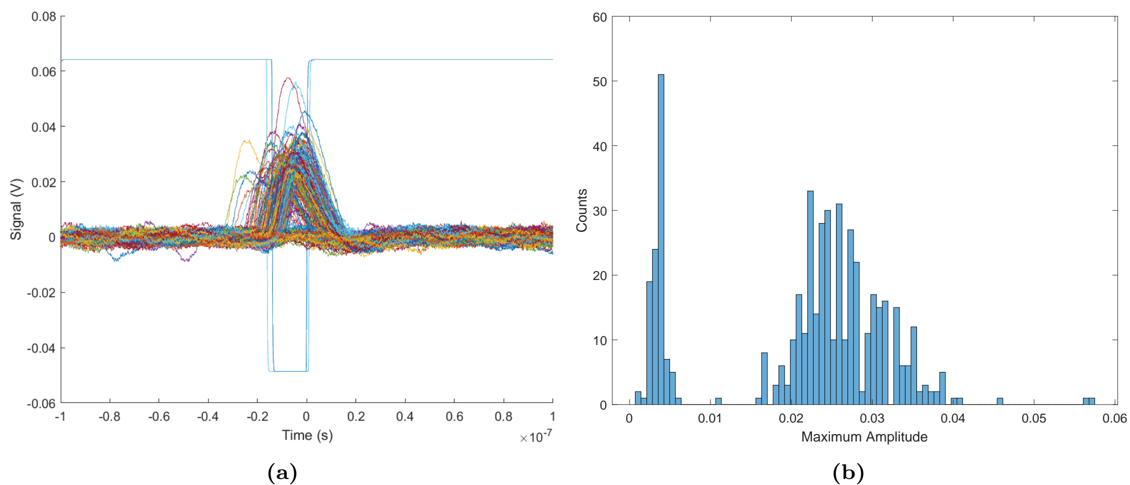

(a) (b)

Figure 6.17: All 500 waveforms (a) collected in position 1 at 1000 V and the distribution of the maximum signal amplitude (b).

The rectangular signals are due to the Keithley. It takes a while for the power supply to become stable after the voltage is changed. These signals are always the first or last waveforms collected in the measurement and should be removed by adding a delay after the voltage change, before the measurement is started. This was tested by adding a 10 s delay after the voltage change. The delay removed almost all rectangular signals. Those that remained are most likely due to saturation or discharges in the electronics, and can easily be removed in the data analysis. The data analysis also uses baseline correction to remove offsets in the signal due to noise in the measurement system. Baseline correction moves the signals to the same

location on the voltage axis and makes the amplitude heights comparable.

One source for the large uncertainty are the flat signals. Figure 6.17b shows the distribution of the signal maximum amplitude. The histogram shows two clear peaks. The peak at low amplitudes is mainly due to noise. In the results presented in this thesis the noise signals have been removed by requiring the maximum amplitude to be larger than 0.01 V. However, this might bias the results because it also removes very small signals. A better method to remove the flat signals would be to select signals based on their shape. Efforts to implement shape selection in the analysis haven't been successful. The next step was to try to reduce the number of flat lines in each measurement. Up to one fifth of the signals can be flat or almost flat. Two methods were tried to reduce the fraction of bad signals, changing the trigger and increasing the number of collected waveforms. The trigger was changed from 26 mV to 35 mV. Changing the trigger did not change the number of flat signals, but it helps to reduce the noise in the signals. The effect of increasing the number of collected waveforms was studied by combining waveforms from several measurements. The test was done with 500, 1000, 1500, 2000 and 2500 waveforms. Increasing the number of collected waveforms had only a small effect on the fraction of flat signals and it didn't reduce the measurement uncertainty. However, collecting more waveforms could help reduce the variation between measurements. Effects on the variation were not studied in this thesis.

The cause of the flat signals is unclear. Somehow the measurement is triggered by the silicon detector even though no signal is generated in the diamond. One theory was that the measurement is triggered by bad signals e.g. due to noise. This was tested by reading both the diamond and the silicon signal from the oscilloscope. The signals from the silicon were good and always above the set trigger level, so bad signals from the silicon can't be the cause of the large uncertainty. Another idea was that the measurement is triggered by surrounding light. The measurements are performed in a dark room and the setup is enclosed in a dark box, so light from outside of the box can not trigger the measurement. The only light source inside the box are the LEDs on the stage controller end switches. But the LEDs are turned on only for a short time during the initialization. Therefore, the measurement can't be triggered by surrounding light. The measurement could be triggered by background radiation or scattered electrons. The box into which the setup is placed, is not well shielded from background radiation, but the metal plate the stage controller is built on top shields the bottom side of the setup. A thin layer of aluminium foil is folded over the detectors in order to stop light and low energy radiation. This shields the

detectors from radiation coming from the top or bottom, but not from the sides. Adding more shielding close to the detectors without affecting the measurement result is challenging, since all shielding between the diamond and the source will also change the energy of the electrons used for the measurement. In the future one could test if adding more shielding to the insides of the box would reduce the number of bad signals.

A large part of the uncertainty is caused by the variation in the signal amplitude. The uncertainty in every position on the averaged signal is affected by the spread (i.e. the standard deviation) of all 500 waveforms in the studied position. Electrons emitted from the source have different energy and energy deposition due to Landau fluctuations and different angles of incidence, so some variation in the signal amplitude is expected. Variation in the signal amplitude can also be a sign of charge trapping. Amplitude variations caused by variations in the electron energy can be reduced by selecting only electrons close to the endpoint energy. This can be done with a suitable collimator. A collimator can also be used to restrict the angle in which the electrons enter the diamond.

7. Conclusions

Different impurities and crystal irregularities affect especially electrical properties of semiconductor materials. Electrical properties of the material define the safe operational region of semiconductor devices, and optimal operation of radiation detectors requires knowledge of charge carrier transport mechanisms and leakage current. Characterization is therefore an important part of designing and fabricating semiconductor detectors. This thesis presents the quality assurance process of CVD diamond detectors for the PPS-detectors in the CMS-experiment. The quality assurance consists of visual inspection with an optical and a cross polarized light microscope, and electrical characterization by leakage current and charge collection efficiency (CCE) measurements. All steps in the quality assurance process are presented, with the main focus being on the CCE measurement. Improvement and testing of the CCE measurement setup is a substantial part in this work.

A stage controller using an Arduino (an electronics board for reading inputs and turning them into outputs controlled by Arduino software) and custom made software based on MATLAB, was built to allow for automatic measurement of CCE in different positions on the diamond detector. The stage controller also makes the measurement safer for the operator since it requires less handling of the radiation source. The setup was tested by measuring the CCE of a reference diamond in five different positions. The reproducibility of the results was checked by doing 20 consecutive measurements with identical settings. The stage controller was successfully used to scan and measure the full sample area. The results were stable over time and similar in the different positions. However, further work needs to be done to reduce the measurement uncertainty and the variation between measurements. The cause of the uncertainty seems to be the variations in the signal shape and height. Rectangular and step like signals could be removed in the signal analysis and by adding a delay after the voltage change. The flat signals could be removed by requiring the signal amplitude to be above a certain level. However, the results might be biased since this also removes signals with small amplitude. Future work will include finding the cause of these signals and reducing their number, as well as development of a method to select signals with a certain shape. One should also check whether

selecting only electrons from the higher end of the energy distribution helps reduce the variation in signal height. The ^{90}Sr-source should be further collimated to allow for a more narrow beam for an even more precise scanning of samples. With the current collimation the width of the electron beam is more than half of the diamond sample side length, so the irradiated area on the diamond sample is large.

In addition, the quality assurance protocol still needs some work for defining final criteria for selecting good diamond detectors. This is the first time the quality assurance of CVD diamond detectors is done on this scale in the Detector Laboratory of University of Helsinki, so there is not yet a clear picture of how the defects observed in the visual inspection affect the electrical properties of the sample, and what are good results. This is the case especially for the visual inspection with a cross polarized light microscope and measurement of charge collection efficiency that do not yet have rejection limits. The correlation between defects and electrical properties will become clearer as more samples are measured and more experience is gained.

Bibliography

1 T Naaranoja, M Golovleva, A Gädda, L Martikainen, J Ott, M Berretti, F Garcia, P Luukka, T Tuuva, and K Österberg. Irradiated single crystal chemical vapor deposition diamond characterized with various ionizing particles. *physica status solidi (a)*, 216(21):1900361, 2019.

2 T Naaranoja, M Golovleva, L Martikainen, M Berretti, and K Österberg. Space charge polarization in irradiated single crystal CVD diamond. *Diamond and Related Materials*, 96:167–175, 2019.

3 G Antchev, P Aspell, I Atanassov, V Avati, J Baechler, V Berardi, M Berretti, E Bossini, U Bottigli, M Bozzo, et al. Diamond detectors for the totem timing upgrade. *Journal of Instrumentation*, 12(03):P03007, 2017.

4 N Minafra. Development of a timing detector for the totem experiment at the LHC. *The European Physical Journal Plus*, 132(9):402, 2017.

5 H Kagan. Recent advances in diamond detector development. *Nuclear Instruments and Methods in Physics Research Section A: Accelerators, Spectrometers, Detectors and Associated Equipment*, 541(1-2):221–227, 2005.

6 G Lindström, M Moll, and E Fretwurst. Radiation hardness of silicon detectors–a challenge from high-energy physics. *Nuclear Instruments and Methods in Physics Research Section A: Accelerators, Spectrometers, Detectors and Associated Equipment*, 426(1):1–15, 1999.

7 H Pernegger, S Roe, P Weilhammer, V Eremin, H Frais-Kölbl, E Griesmayer, H Kagan, Stephen Schnetzer, R Stone, W Trischuk, et al. Charge-carrier properties in synthetic single-crystal diamond measured with the transient-current technique. *Journal of Applied Physics*, 97(7):073704, 2005.

8 E Bossini. The CMS precision proton spectrometer timing system: performance

in run 2, future upgrades and sensor radiation hardness studies. *Proceedings of the IPRD2019 Conference, arXiv:2004.11068*, 2020.

9 G Antchev, P Aspell, I Atanassov, et al. Timing performance of a double layer diamond detector. 2017. https://iopscience.iop.org/article/10.1088/1748-0221/12/03/P03026.

10 G Lutz. *Semiconductor radiation detectors : device physics.* Springer, Berlin, 1999.

11 G F. Knoll. *Radiation detection and measurement.* John Wiley, Hoboken, N.J., 4th edition, 2010.

12 M Franklin, A Fry, KK Gan, S Han, H Kagan, S Kanda, D Kania, R Kass, SK Kim, R Malchow, et al. Development of diamond radiation detectors for SSC and LHC. *Nuclear Instruments and Methods in Physics Research Section A: Accelerators, Spectrometers, Detectors and Associated Equipment*, 315(1-3):39–42, 1992.

13 M Friedl. Diamond detectors for ionizing radiation. *Diploma thesis*, 1999. http://www.hephy.at/user/friedl/da/da.pdf, Accessed 2020-05-19.

14 RJ Tapper. Diamond detectors in particle physics. *Reports on progress in Physics*, 63(8):1273, 2000.

15 M Pomorski. Electronic properties of single crystal CVD diamond and its suitability for particle detection in hadron physics experiments. *Wolfgang von Goethe University, Frankfurt am Main, Germany*, 2008.

16 P S Myung. Fabrication and characterization of bulk diamond radiation detectors. *BSc honours project report*, 2017. https://www.physics.nus.edu.sg/student/Honours%20Projects%20Repository%202016-17/Park%20Sun%20Myung.pdf, Accessed 2020-05-19.

17 H Pernegger. High mobility diamonds and particle detectors. *physica status solidi (a)*, 203(13):3299–3314, 2006.

18 DR Kania, MI Landstrass, MA Plano, LS Pan, and S Han. Diamond radiation detectors. *Diamond and Related Materials*, 2(5-7):1012–1019, 1993.

19 D K Schroder. *Semiconductor material and device characterization.* John Wiley & Sons, 2015.

20 M Pomorski, E Berdermann, M Ciobanu, A Martemyianov, P Moritz, M Rebisz, and B Marczewska. Characterisation of single crystal CVD diamond particle detectors for hadron physics experiments. *Physica status solidi (a)*, 202(11):2199–2205, 2005.

21 S Ramo. Currents induced by electron motion. *Proceedings of the IRE*, 27(9):584–585, 1939.

22 W Shockley. Currents to conductors induced by a moving point charge. *Journal of applied physics*, 9(10):635–636, 1938.

23 SF Kozlov, E Belcarz, M Hage-Ali, R Stuck, and P Siffert. Diamond nuclear radiation detectors. *Nuclear Instruments and Methods*, 117(1):277–283, 1974.

24 G Kramberger, M Mikuz, M Zavrtanik, I Mandic, V Cindro, and A Gorisek. Effects of bias voltage during priming on operation of diamond detectors. *Proceedings of 21st International Workshop on Vertex Detectors, PoS (Vertex 2012)*, page 013, 2013.

25 M Mathes, M Cristinziani, H Kagan, S Smith, W Trischuk, J Velthuis, and N Wermes. Characterization of a single crystal diamond pixel detector in a high energy particle beam. *Journal of Instrumentation*, 3(12):P12002, 2008.

26 H B Prosper and M Danilov. *Techniques and concepts of high-energy physics XII*, volume 123. Springer Science & Business Media, 2003.

27 J Liu, J Chang, J Zhang, G Zhong, X Liu, X Pang, and J Jia. Design, fabrication and testing of CVD diamond detectors with high performance. *AIP Advances*, 9(4):045205, 2019.

28 Element Six. The element six CVD diamond handbook. *Element Six Technologies*, 5(5.4):1, 2017. https://e6cvd.com/media/wysiwyg/pdf/E6_CVD_Diamond_Handbook_A5_v10X.pdf, Accessed 2020-05-20.

29 P W May. Diamond thin films: a 21st-century material. *Philosophical Transactions of the Royal Society of London. Series A: Mathematical, Physical and Engineering Sciences*, 358(1766):473–495, 2000.

30 RS Balmer, JR Brandon, SL Clewes, HK Dhillon, JM Dodson, I Friel, PN Inglis, TD Madgwick, ML Markham, TP Mollart, et al. Chemical vapour deposition synthetic diamond: materials, technology and applications. *Journal of Physics: Condensed Matter*, 21(36):364221, 2009.

31 JW Morris. Defects in crystals. *Materials Science*, pages 76–107, 2007.

32 W D Callister. *Materials science and engineering : an introduction*. John Wiley, Hoboken, NJ, SI version, 8th edition, 2011.

33 HA Hoff, GL Waytena, CL Vold, JS Suehle, IP Isaacson, ML Rebbert, DI Ma, and K Harris. Ohmic contacts to semiconducting diamond using a Ti/Pt/Au trilayer metallization scheme. *Diamond and related materials*, 5(12):1450–1456, 1996.

34 W Adam, C Bauer, E Berdermann, P Bergonzo, F Bogani, E Borchi, A Brambilla, M Bruzzi, C Colledani, J Conway, et al. Review of the development of diamond radiation sensors. *Nuclear Instruments and Methods in Physics Research Section A: Accelerators, Spectrometers, Detectors and Associated Equipment*, 434(1):131–145, 1999.

35 P Bergonzo, A Brambilla, D Tromson, C Mer, B Guizard, F Foulon, and V Amosov. CVD diamond for radiation detection devices. *Diamond and related materials*, 10(3-7):631–638, 2001.

36 R J Keddy and T L Nam. Diamond radiation detectors. *Radiation Physics and Chemistry*, 41(4-5):767–773, 1993.

37 C M Breeding and J E Shigley. The ”type” classification system of diamonds and its importance in gemology. *Gems & Gemology*, 45(2):96–111, 2009.

38 M Friedl, W Adam, C Bauer, E Berdermann, P Bergonzo, F Bogani, E Borchi, A Brambilla, M Bruzzi, C Colledani, et al. CVD diamond detectors for ionizing radiation. *Nuclear Instruments and Methods in Physics Research Section A: Accelerators, Spectrometers, Detectors and Associated Equipment*, 435(1-2):194–201, 1999.

39 M Schwander and K Partes. A review of diamond synthesis by CVD processes. *Diamond and related materials*, 20(9):1287–1301, 2011.

40 T Tachibana, BE Williams, and JT Glass. Correlation of the electrical properties of metal contacts on diamond films with the chemical nature of the metal-diamond interface. II. Titanium contacts: A carbide-forming metal. *Physical Review B*, 45(20):11975, 1992.

41 M Werner. Diamond metallization for device applications. *Semiconductor science and technology*, 18(3):S41, 2003.

42 H J Queisser and E E Haller. Defects in semiconductors: some fatal, some vital. *Science*, 281(5379):945–950, 1998.

43 M-A Pinault-Thaury, T Tillocher, N Habka, D Kobor, F Jomard, J Chevallier, and J Barjon. n-type CVD diamond: Epitaxy and doping. *Materials Science and Engineering: B*, 176(17):1401–1408, 2011.

44 P W Anderson. Local moments and localized states. *Reviews of Modern Physics*, 50(2):191, 1978.

45 H Pernegger, S Roe, P Weilhammer, V Eremin, H Frais-Kölbl, E Griesmayer, H Kagan, Stephen Schnetzer, R Stone, W Trischuk, et al. Charge-carrier properties in synthetic single-crystal diamond measured with the transient-current technique. *Journal of Applied Physics*, 97(7):073704, 2005.

46 V Eremin, N Strokan, E Verbitskaya, and Z Li. Development of transient current and charge techniques for the measurement of effective net concentration of ionized charges (Neff) in the space charge region of pn junction detectors. *Nuclear Instruments and Methods in Physics Research Section A: Accelerators, Spectrometers, Detectors and Associated Equipment*, 372(3):388–398, 1996.

47 S Zhao. Characterization of the electrical properties of polycrystalline diamond films. *The Ohio State University*, 1994.

48 Laboratoire National Henri Becquerel Recommended data. `http://www.nucleide.org/DDEP_WG/DDEPdata.htm`. Accessed 2020-03-26.

49 What is Arduino?, Arduino web page. `https://www.arduino.cc/en/guide/introduction`. Accessed 2020-05-31.

50 J Mandel. *The statistical analysis of experimental data.* Dover, New York, 1984. Reprint. Originally published, New York, Interscience, 1964., `http://www.loc.gov/catdir/description/dover033/83020599.html`.

A. Stage controller

The stage controller consists of a 2D-stage to hold the sample, two micro stepper motors, one for moving the stage in x-direction and another for moving in the y-direction, two encoders and two end switches. The stepper motors are controlled using A4988 stepper motor drivers connected to an Arduino Uno board. The step size was set to the smallest size possible (1/16) to allow selection of the measurement position with µm precision. The movements of the stage controller are controlled with Arduino and custom made software based on MATLAB.

Encoders attached to the gear wheels connecting the stepper motors and the stage are used to check how much the stepper motors have moved and how stable they are. When the stage controller moves, the Arduino program counts how many steps each motor has moved, as well as the number of times the encoder status has changed, i.e. how many times the light has changed from blocked to unblocked or from unblocked to blocked. Then the program uses the counted number of motor steps to calculate how many times the encoder status is expected to change, knowing that the status changes 16 times in one revolution (3200 steps). The calculated and counted number of changes in the encoder status are compared and a warning is printed if the values don't match.

End switches are installed on two sides of the stage to guarantee that the zero position is the same at the beginning of every measurement. When the stage controller is turned on and the connection between Arduino and MATLAB is opened, the stage controller moves in the x-direction until the switch is turned on and then back until the switch is turned off. The position at which the switch is turned off again is set as the zero position in the x-direction. The same procedure is repeated for the other stepper motor to find the zero point in the y-direction.

The sending of the measurement position coordinates and the data acquisition is handled by custom made MATLAB software. A custom made Graphical User Interface (GUI) is used to select how many of the defined positions are measured, or to select and measure a completely new position. The GUI also displays the current position of the stage controller. The measurement positions are calculated by the program from the sample dimensions defined by the user. The program can

be used to scan one or several samples in one run. There are two measurement geometries, ”Measure5” and ”Measure16”. Geometry ”Measure16” is made to scan 4×4 array of measurement points, but can be used to scan any $n \times n$ array of measurement points, n being the number of measurement points on each side. For 16 measurement points one can also choose to scan only one position, row or column for each sample. Geometry ”Measure5” is made for measuring five positions on the sample, one in every corner and one in the center. However, the geometry can be used to measure other sets of measurement positions. In this case the user writes the x- and y-coordinates in separate arrays in the order they should be measured.

The movement of the stage and the measurement are handled by Arduino and MATLAB in the following manner. First MATLAB converts both the x- and y-coordinate from mm to motor steps and combines them to a string which is sent over the serial to Arduino. Arduino reads the string, splits it to a x and y component, and moves both stepper motors according to the coordinates. When the stage controller is at the right position Arduino sends a string back to MATLAB to tell that it is ready. MATLAB calls the measurement script and connects to the oscilloscope and the voltage source of the sample. The measurement procedure and parameters are defined by the user in the measurement script. MATLAB redoes the measurement once if the first try ends in an error. The measurement position is skipped in case both measurements fail. This process is repeated until all selected positions have been measured. When the scanning is complete MATLAB prints the total number of steps and encoder counts for the scan and checks if the values match.

B. Reproducibility measurements

This appendix presents the results of the reproducibility measurements. The mean is calculated from all 20 measurements. σ is the uncertainty of the mean. Std is the standard deviation of the parameter and describes how the parameter fluctuates around its mean.

Table B.1: Maximum signal amplitude.

	Position 1			Position 2		
V [V]	Mean [mV]	σ [mV]	Std [mV]	Mean [mV]	σ [mV]	Std [mV]
100	19.488	0.072	0.500	19.163	0.070	0.525
200	20.993	0.072	0.773	20.973	0.070	0.671
300	21.456	0.072	1.032	21.149	0.070	0.909
400	21.654	0.072	1.074	21.320	0.070	0.836
500	21.345	0.072	1.040	21.546	0.070	1.066
600	21.297	0.072	1.222	21.215	0.070	1.103
700	21.311	0.072	1.147	21.821	0.070	0.764
800	21.155	0.072	1.070	21.526	0.070	0.881
900	21.171	0.072	1.212	21.568	0.070	0.925
1000	20.816	0.072	1.179	21.217	0.070	1.100

	Position 3			Position 4		
V [V]	Mean [mV]	σ [mV]	Std [mV]	Mean [mV]	σ [mV]	Std [mV]
100	19.276	0.071	0.417	19.012	0.073	0.540
200	20.993	0.071	0.883	20.937	0.073	0.591
300	21.821	0.071	0.753	21.366	0.073	0.865
400	21.142	0.071	0.749	21.259	0.073	0.897
500	21.390	0.071	1.066	21.021	0.073	0.919
600	21.866	0.071	0.944	21.260	0.073	1.024
700	21.366	0.071	0.943	21.309	0.073	1.035
800	21.419	0.071	1.022	21.052	0.073	1.249
900	21.525	0.071	1.131	21.138	0.073	1.079
1000	21.314	0.071	1.094	21.164	0.073	1.108

	Position 5		
V [V]	Mean [mV]	σ [mV]	Std [mV]
100	19.224	0.072	0.504
200	20.707	0.072	0.723
300	20.957	0.072	0.896
400	21.665	0.072	0.779
500	20.913	0.072	0.916
600	21.291	0.072	0.906
700	21.290	0.072	1.165
800	21.158	0.072	0.897
900	21.406	0.072	1.018
1000	21.003	0.072	1.123

Table B.2: Charge carrier velocity.

	Position 1		
V [V]	Mean [µm/s]	σ [µm/s]	Std [µm/s]
100	$1.7475 \cdot 10^{10}$	$0.0040 \cdot 10^{10}$	$0.0300 \cdot 10^{10}$
200	$1.8738 \cdot 10^{10}$	$0.0044 \cdot 10^{10}$	$0.0282 \cdot 10^{10}$
300	$1.9017 \cdot 10^{10}$	$0.0049 \cdot 10^{10}$	$0.0341 \cdot 10^{10}$
400	$1.9271 \cdot 10^{10}$	$0.0052 \cdot 10^{10}$	$0.0457 \cdot 10^{10}$
500	$1.9143 \cdot 10^{10}$	$0.0051 \cdot 10^{10}$	$0.0479 \cdot 10^{10}$
600	$1.9329 \cdot 10^{10}$	$0.0054 \cdot 10^{10}$	$0.0513 \cdot 10^{10}$
700	$1.9521 \cdot 10^{10}$	$0.0055 \cdot 10^{10}$	$0.0568 \cdot 10^{10}$
800	$1.9405 \cdot 10^{10}$	$0.0055 \cdot 10^{10}$	$0.0660 \cdot 10^{10}$
900	$1.9646 \cdot 10^{10}$	$0.0053 \cdot 10^{10}$	$0.0560 \cdot 10^{10}$
1000	$1.9661 \cdot 10^{10}$	$0.0060 \cdot 10^{10}$	$0.5494 \cdot 10^{10}$

	Position 2		
V [V]	Mean [µm/s]	σ [µm/s]	Std [µm/s]
100	$1.7236 \cdot 10^{10}$	$0.0041 \cdot 10^{10}$	$0.0258 \cdot 10^{10}$
200	$1.8643 \cdot 10^{10}$	$0.0045 \cdot 10^{10}$	$0.0520 \cdot 10^{10}$
300	$1.8977 \cdot 10^{10}$	$0.0051 \cdot 10^{10}$	$0.0415 \cdot 10^{10}$
400	$1.9194 \cdot 10^{10}$	$0.0049 \cdot 10^{10}$	$0.0386 \cdot 10^{10}$
500	$1.9229 \cdot 10^{10}$	$0.0053 \cdot 10^{10}$	$0.0429 \cdot 10^{10}$
600	$1.9328 \cdot 10^{10}$	$0.0052 \cdot 10^{10}$	$0.0560 \cdot 10^{10}$
700	$1.9566 \cdot 10^{10}$	$0.0051 \cdot 10^{10}$	$0.0560 \cdot 10^{10}$
800	$1.9537 \cdot 10^{10}$	$0.0051 \cdot 10^{10}$	$0.0592 \cdot 10^{10}$
900	$1.9597 \cdot 10^{10}$	$0.0054 \cdot 10^{10}$	$0.0409 \cdot 10^{10}$
1000	$1.9387 \cdot 10^{10}$	$0.0053 \cdot 10^{10}$	$0.0379 \cdot 10^{10}$

	Position 3		
V [V]	Mean [µm/s]	σ [µm/s]	Std [µm/s]
100	$1.7349 \cdot 10^{10}$	$0.0038 \cdot 10^{10}$	$0.0338 \cdot 10^{10}$
200	$1.8666 \cdot 10^{10}$	$0.0050 \cdot 10^{10}$	$0.0327 \cdot 10^{10}$
300	$1.9145 \cdot 10^{10}$	$0.0048 \cdot 10^{10}$	$0.0353 \cdot 10^{10}$
400	$1.9263 \cdot 10^{10}$	$0.0052 \cdot 10^{10}$	$0.0363 \cdot 10^{10}$
500	$1.9354 \cdot 10^{10}$	$0.0050 \cdot 10^{10}$	$0.0294 \cdot 10^{10}$
600	$1.9437 \cdot 10^{10}$	$0.0052 \cdot 10^{10}$	$0.0559 \cdot 10^{10}$
700	$1.9516 \cdot 10^{10}$	$0.0054 \cdot 10^{10}$	$0.0484 \cdot 10^{10}$
800	$1.9385 \cdot 10^{10}$	$0.0055 \cdot 10^{10}$	$0.0633 \cdot 10^{10}$
900	$1.9637 \cdot 10^{10}$	$0.0051 \cdot 10^{10}$	$0.0442 \cdot 10^{10}$
1000	$1.9549 \cdot 10^{10}$	$0.0052 \cdot 10^{10}$	$0.0451 \cdot 10^{10}$

	Position 4		
V [V]	Mean [µm/s]	σ [µm/s]	Std [µm/s]
100	$1.7260 \cdot 10^{10}$	$0.0041 \cdot 10^{10}$	$0.0340 \cdot 10^{10}$
200	$1.8580 \cdot 10^{10}$	$0.0046 \cdot 10^{10}$	$0.0361 \cdot 10^{10}$
300	$1.8933 \cdot 10^{10}$	$0.0050 \cdot 10^{10}$	$0.0542 \cdot 10^{10}$
400	$1.8971 \cdot 10^{10}$	$0.0050 \cdot 10^{10}$	$0.0258 \cdot 10^{10}$
500	$1.9499 \cdot 10^{10}$	$0.0053 \cdot 10^{10}$	$0.0440 \cdot 10^{10}$
600	$1.9192 \cdot 10^{10}$	$0.0052 \cdot 10^{10}$	$0.0569 \cdot 10^{10}$
700	$1.9294 \cdot 10^{10}$	$0.0054 \cdot 10^{10}$	$0.0275 \cdot 10^{10}$
800	$1.9432 \cdot 10^{10}$	$0.0052 \cdot 10^{10}$	$0.0537 \cdot 10^{10}$
900	$1.9442 \cdot 10^{10}$	$0.0053 \cdot 10^{10}$	$0.0651 \cdot 10^{10}$
1000	$1.9432 \cdot 10^{10}$	$0.0053 \cdot 10^{10}$	$0.0536 \cdot 10^{10}$

	Position 5		
V [V]	Mean [µm/s]	σ [µm/s]	Std [µm/s]
100	$1.7312 \cdot 10^{10}$	$0.0040 \cdot 10^{10}$	$0.0171 \cdot 10^{10}$
200	$1.8641 \cdot 10^{10}$	$0.0046 \cdot 10^{10}$	$0.0313 \cdot 10^{10}$
300	$1.8931 \cdot 10^{10}$	$0.0048 \cdot 10^{10}$	$0.0350 \cdot 10^{10}$
400	$1.9187 \cdot 10^{10}$	$0.0048 \cdot 10^{10}$	$0.0410 \cdot 10^{10}$
500	$1.9172 \cdot 10^{10}$	$0.0052 \cdot 10^{10}$	$0.0602 \cdot 10^{10}$
600	$1.9426 \cdot 10^{10}$	$0.0052 \cdot 10^{10}$	$0.0414 \cdot 10^{10}$
700	$1.9354 \cdot 10^{10}$	$0.0052 \cdot 10^{10}$	$0.0284 \cdot 10^{10}$
800	$1.9506 \cdot 10^{10}$	$0.0055 \cdot 10^{10}$	$0.0436 \cdot 10^{10}$
900	$1.9386 \cdot 10^{10}$	$0.0051 \cdot 10^{10}$	$0.0529 \cdot 10^{10}$
1000	$1.9591 \cdot 10^{10}$	$0.0053 \cdot 10^{10}$	$0.0535 \cdot 10^{10}$

Table B.4: Collected charge.

	Position 1		
V [V]	Mean [C]	σ [C]	Std [C]
100	$3.6617 \cdot 10^{-10}$	$0.0069 \cdot 10^{-10}$	$0.2512 \cdot 10^{-10}$
200	$3.7446 \cdot 10^{-10}$	$0.0067 \cdot 10^{-10}$	$0.1912 \cdot 10^{-10}$
300	$3.7750 \cdot 10^{-10}$	$0.0068 \cdot 10^{-10}$	$0.1860 \cdot 10^{-10}$
400	$3.7801 \cdot 10^{-10}$	$0.0066 \cdot 10^{-10}$	$0.2485 \cdot 10^{-10}$
500	$3.7752 \cdot 10^{-10}$	$0.0067 \cdot 10^{-10}$	$0.2153 \cdot 10^{-10}$
600	$3.7804 \cdot 10^{-10}$	$0.0069 \cdot 10^{-10}$	$0.2486 \cdot 10^{-10}$
700	$3.5912 \cdot 10^{-10}$	$0.0067 \cdot 10^{-10}$	$0.1913 \cdot 10^{-10}$
800	$3.7964 \cdot 10^{-10}$	$0.0068 \cdot 10^{-10}$	$0.2071 \cdot 10^{-10}$
900	$3.6809 \cdot 10^{-10}$	$0.0068 \cdot 10^{-10}$	$0.3075 \cdot 10^{-10}$
1000	$3.7133 \cdot 10^{-10}$	$0.0066 \cdot 10^{-10}$	$0.1872 \cdot 10^{-10}$

	Position 2		
V [V]	Mean [C]	σ [C]	Std [C]
100	$3.7340 \cdot 10^{-10}$	$0.0069 \cdot 10^{-10}$	$0.2232 \cdot 10^{-10}$
200	$3.7394 \cdot 10^{-10}$	$0.0067 \cdot 10^{-10}$	$0.2711 \cdot 10^{-10}$
300	$3.6808 \cdot 10^{-10}$	$0.0067 \cdot 10^{-10}$	$0.2295 \cdot 10^{-10}$
400	$3.6899 \cdot 10^{-10}$	$0.0067 \cdot 10^{-10}$	$0.2143 \cdot 10^{-10}$
500	$3.8203 \cdot 10^{-10}$	$0.0067 \cdot 10^{-10}$	$0.1978 \cdot 10^{-10}$
600	$3.7366 \cdot 10^{-10}$	$0.0067 \cdot 10^{-10}$	$0.2617 \cdot 10^{-10}$
700	$3.7892 \cdot 10^{-10}$	$0.0068 \cdot 10^{-10}$	$0.1391 \cdot 10^{-10}$
800	$3.6980 \cdot 10^{-10}$	$0.0067 \cdot 10^{-10}$	$0.2673 \cdot 10^{-10}$
900	$3.6743 \cdot 10^{-10}$	$0.0066 \cdot 10^{-10}$	$0.1387 \cdot 10^{-10}$
1000	$3.6912 \cdot 10^{-10}$	$0.0067 \cdot 10^{-10}$	$0.2482 \cdot 10^{-10}$

	Position 3		
V [V]	Mean [C]	σ [C]	Std [C]
100	$3.7008 \cdot 10^{-10}$	$0.0072 \cdot 10^{-10}$	$0.2133 \cdot 10^{-10}$
200	$3.7570 \cdot 10^{-10}$	$0.0068 \cdot 10^{-10}$	$0.2591 \cdot 10^{-10}$
300	$3.7820 \cdot 10^{-10}$	$0.0069 \cdot 10^{-10}$	$0.2072 \cdot 10^{-10}$
400	$3.7579 \cdot 10^{-10}$	$0.0068 \cdot 10^{-10}$	$0.1679 \cdot 10^{-10}$
500	$3.6683 \cdot 10^{-10}$	$0.0069 \cdot 10^{-10}$	$0.2019 \cdot 10^{-10}$
600	$3.7177 \cdot 10^{-10}$	$0.0068 \cdot 10^{-10}$	$0.1644 \cdot 10^{-10}$
700	$3.6857 \cdot 10^{-10}$	$0.0068 \cdot 10^{-10}$	$0.2409 \cdot 10^{-10}$
800	$3.8211 \cdot 10^{-10}$	$0.0067 \cdot 10^{-10}$	$0.2887 \cdot 10^{-10}$
900	$3.6639 \cdot 10^{-10}$	$0.0068 \cdot 10^{-10}$	$0.2417 \cdot 10^{-10}$
1000	$3.6195 \cdot 10^{-10}$	$0.0067 \cdot 10^{-10}$	$0.2596 \cdot 10^{-10}$

	Position 4		
V [V]	Mean [C]	σ [C]	Std [C]
100	$3.6453 \cdot 10^{-10}$	$0.0069 \cdot 10^{-10}$	$0.1820 \cdot 10^{-10}$
200	$3.7764 \cdot 10^{-10}$	$0.0069 \cdot 10^{-10}$	$0.2209 \cdot 10^{-10}$
300	$3.8216 \cdot 10^{-10}$	$0.0068 \cdot 10^{-10}$	$0.2328 \cdot 10^{-10}$
400	$3.7276 \cdot 10^{-10}$	$0.0066 \cdot 10^{-10}$	$0.1536 \cdot 10^{-10}$
500	$3.6327 \cdot 10^{-10}$	$0.0066 \cdot 10^{-10}$	$0.2486 \cdot 10^{-10}$
600	$3.7528 \cdot 10^{-10}$	$0.0066 \cdot 10^{-10}$	$0.1854 \cdot 10^{-10}$
700	$3.7869 \cdot 10^{-10}$	$0.0066 \cdot 10^{-10}$	$0.1852 \cdot 10^{-10}$
800	$3.6662 \cdot 10^{-10}$	$0.0066 \cdot 10^{-10}$	$0.2633 \cdot 10^{-10}$
900	$3.7838 \cdot 10^{-10}$	$0.0065 \cdot 10^{-10}$	$0.1914 \cdot 10^{-10}$
1000	$3.7169 \cdot 10^{-10}$	$0.0066 \cdot 10^{-10}$	$0.1581 \cdot 10^{-10}$

	Position 5		
V [V]	Mean [C]	σ [C]	Std [C]
100	$3.7128 \cdot 10^{-10}$	$0.0071 \cdot 10^{-10}$	$0.2168 \cdot 10^{-10}$
200	$3.6915 \cdot 10^{-10}$	$0.0068 \cdot 10^{-10}$	$0.1495 \cdot 10^{-10}$
300	$3.7362 \cdot 10^{-10}$	$0.0067 \cdot 10^{-10}$	$0.1772 \cdot 10^{-10}$
400	$3.6836 \cdot 10^{-10}$	$0.0068 \cdot 10^{-10}$	$0.2265 \cdot 10^{-10}$
500	$3.7069 \cdot 10^{-10}$	$0.0068 \cdot 10^{-10}$	$0.2143 \cdot 10^{-10}$
600	$3.7325 \cdot 10^{-10}$	$0.0067 \cdot 10^{-10}$	$0.1748 \cdot 10^{-10}$
700	$3.8230 \cdot 10^{-10}$	$0.0068 \cdot 10^{-10}$	$0.2123 \cdot 10^{-10}$
800	$3.7946 \cdot 10^{-10}$	$0.0069 \cdot 10^{-10}$	$0.2007 \cdot 10^{-10}$
900	$3.7793 \cdot 10^{-10}$	$0.0067 \cdot 10^{-10}$	$0.1992 \cdot 10^{-10}$
1000	$3.6946 \cdot 10^{-10}$	$0.0068 \cdot 10^{-10}$	$0.1681 \cdot 10^{-10}$

Table B.6: Charge collection efficiency.

	Position 1			Position 2		
V [V]	Mean [%]	σ [%]	Std [%]	Mean [%]	σ [%]	Std [%]
100	98.06	1.17	6.73	100.00	1.18	5.98
200	99.62	1.13	5.42	98.88	1.13	7.10
300	99.07	1.12	5.24	97.05	1.10	5.65
400	100.46	1.12	6.80	98.04	1.11	5.60
500	98.97	1.10	5.84	100.49	1.11	4.78
600	99.69	1.13	6.00	98.84	1.11	6.92
700	94.73	1.08	5.87	99.33	1.10	3.64
800	100.14	1.11	5.45	96.82	1.08	7.02
900	97.62	1.11	8.43	97.54	1.09	3.62
1000	99.90	1.12	5.04	99.31	1.13	6.68

	Position 3			Position 4		
V [V]	Mean [%]	σ [%]	Std [%]	Mean [%]	σ [%]	Std [%]
100	99.81	1.20	4.24	96.95	1.17	5.92
200	98.84	1.15	6.01	99.85	1.15	5.83
300	99.19	1.13	5.34	100.49	1.13	5.70
400	98.89	1.13	4.34	99.16	1.11	4.05
500	96.52	1.11	5.16	95.68	1.07	6.54
600	98.67	1.12	4.11	99.33	1.11	4.98
700	96.16	1.10	6.46	98.96	1.09	4.77
800	100.00	1.11	7.56	96.12	1.08	6.85
900	97.30	1.11	6.65	99.77	1.09	5.05
1000	97.62	1.12	6.96	100.18	1.12	3.92

	Position 5		
V [V]	Mean [%]	σ [%]	Std [%]
100	99.43	1.20	5.81
200	97.44	1.13	4.43
300	97.27	1.11	5.07
400	96.87	1.12	6.28
500	96.05	1.08	5.28
600	98.11	1.11	5.12
700	99.47	1.11	6.12
800	98.25	1.12	5.20
900	99.30	1.11	5.85
1000	99.40	1.14	4.52